FISCHER--TROPSCH SYNTHESIS OVER A RUTHENIUM CATALYST: INFRARED AND KINETIC STUDIES

CALIFORNIA UNIV., BERKELEY. LAWRENCE BERKELEY LAB

APR 1979

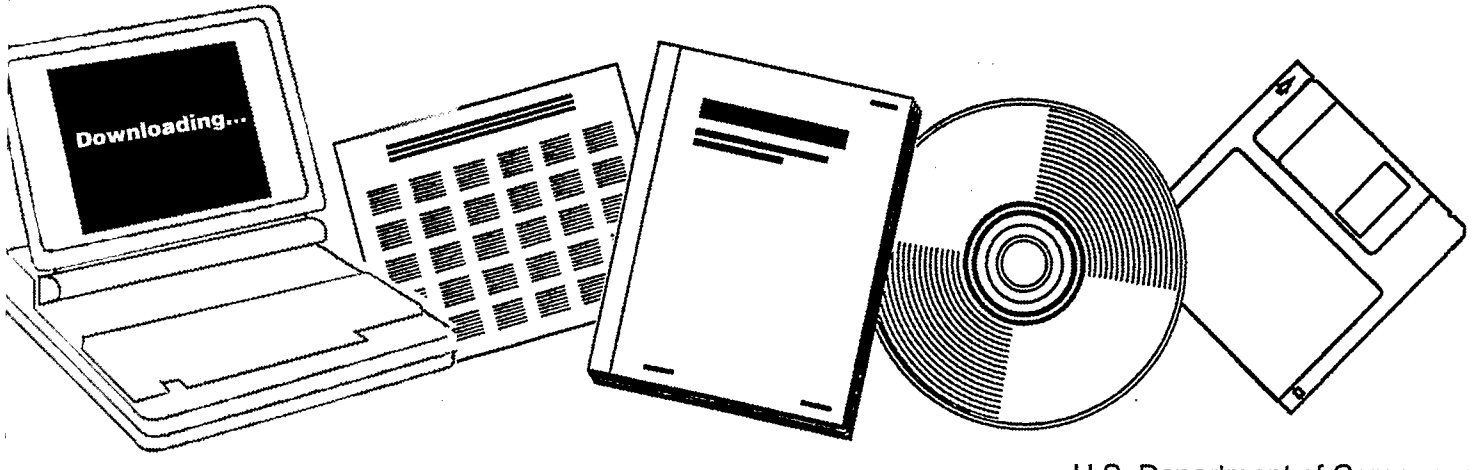

One Source. One Search. One Solution.

NTIS

Providing Permanent, Easy Access to U.S. Government Information

National Technical Information Service is the nation's largest repository and disseminator of government-initiated scientific, technical, engineering, and related business information. The NTIS collection includes almost 3,000,000 information products in a variety of formats: electronic download, online access, CD-ROM, magnetic tape, diskette, multimedia, microfiche and paper.

Search the NTIS Database from 1990 forward

NTIS has upgraded its bibliographic database system and has made all entries since 1990 searchable on **www.ntis.gov.** You now have access to information on more than 600,000 government research information products from this web site.

Link to Full Text Documents at Government Web Sites

Because many Government agencies have their most recent reports available on their own web site, we have added links directly to these reports. When available, you will see a link on the right side of the bibliographic screen.

Download Publications (1997 - Present)

NTIS can now provides the full text of reports as downloadable PDF files. This means that when an agency stops maintaining a report on the web, NTIS will offer a downloadable version. There is a nominal fee for each download for most publications.

For more information visit our website:

www.ntis.gov

U.S. DEPARTMENT OF COMMERCE
Technology Administration
National Technical Information Service
Springfield, VA 22161

FISCHER-TROPSCH SYNTHESIS OVER A RUTHENIUM CATALYST: INFRARED AND KINETIC STUDIES

John G. Ekerdt
(Ph. D. thesis)

April 1979

Prepared for the U. S. Department of Energy
under Contract W-7405-ENG-48

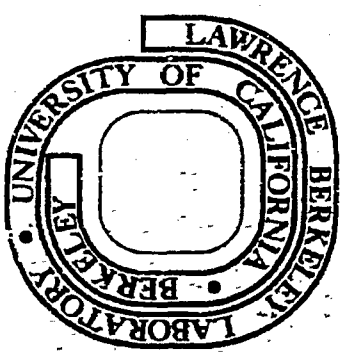

BLANK PAGE

Fischer-Tropsch Synthesis Over a Ruthenium Catalyst: Infrared and Kinetic Studies

John G. Ekerdt
Materials and Molecular Research Division
Lawrence Berkeley Laboratory

and

Department of Chemical Engineering
University of California, Berkeley, CA 94709

ABSTRACT

The synthesis of hydrocarbons from CO and H_2 was studied on a silica-supported Ru catalyst and the species present on the catalyst surface were characterized by infrared spectroscopy. Initial rates of methane formation were correlated by the expression $N_{CH_4} = 7.4 \times 10^5 \exp(-24{,}000/RT)\ P_{H_2}^{1.5}/P_{CO}^{0.6}$. The synthesis of ethane, propylene, and propane, the principle products observed in addition to methane, were favored at high CO partial pressures, low H_2/CO ratios, and low temperatures. The primary feature observed in the infrared spectra was a band at 2030 cm^{-1}, associated with chemisorbed CO. Neither the position nor intensity of this band was affected by the CO partial pressure or the H_2/CO ratio. The CO band intensity did decrease with increasing temperature due to a decrease in CO coverage. Bands were also observed at 2950, 2910, and 2845 cm^{-1} and were assigned to hydrocarbon structures surrounded by chemisorbed CO. These structures could be removed from the catalyst surface by hydrogenation, but do not appear to be

BLANK PAGE

intermediates in the synthesis of stable products. Reduction of the catalyst following steady-state reaction revealed that the working catalyst maintains a reservoir of carbon several Ru monolayers in magnitude. A part of the carbon appears to be dissolved in the Ru, but all of it readily reacts with H_2 to form methane, ethane, and propane in the absence of chemisorbed CO.

Evidence obtained from the combined infrared and kinetic studies suggests that the first stage of reaction involves the dissociation of CO to produce surface carbon atoms. Hydrogenation of the surface carbon to ethane and propane in the absence of chemisorbed CO suggests that chain propagation does not involve CO insertion into a metal-alkyl type intermediate. In an attempt to identify reaction intermediates, ethylene and cyclohexene were added to the synthesis gas feed. In the case of ethylene enhanced yields of propylene were observed. When cyclohexene was used as a scavenger a series of alkyl cyclohexene and alkyl cyclohexane products were obtained. The results of both experiments suggest that alkylidene groups are present on the catalyst surface.

Reaction mechanisms for the formation of methane are developed and used to formulate methanation rate expressions which are consistent with the experimental observations. In addition, reaction mechanisms for the formation of higher molecular weight olefins and alkanes are proposed which incorporate the postulated alkylidenes in chain growth as well as chain termination steps.

A. T. Bell

TABLE OF CONTENTS

LIST OF TABLES

LIST OF FIGURES

I. INTRODUCTION AND LITERATURE REVIEW

A. Introduction

Alternate sources of fuels and chemical feedstocks need to be developed due to the onset of decreasing domestic crude oil supplies. The gasification of coal, an abundant resource, produces H_2 and CO which can be reacted by Fischer-Tropsch synthesis to produce hydrocarbons. The basic mechanisms underlying the synthesis reaction are the subject of active research. Factors controlling Fischer-Tropsch catalyst activity and selectivity need to be better identified and understood to aid in the ultimate development of a viable alternate fuel and chemical supply.

The purpose of this work was to develop a better understanding of the elementary processes involved in the reaction of H_2 and CO to form synthesis products over a silica-supported Ru catalyst. Ruthenium was chosen for study because it is the most active of the transition metal catalysts and because Ru catalyzed hydrocarbon products are primarily straight-chain and non-oxygenated. The investigative approach involved the measurement of synthesis rates; the recording of infrared spectra of adsorbed surface species, under reaction conditions; and the addition of olefins to scavenge reaction intermediates.

B. Literature Review

1. General

Fischer-Tropsch synthesis of hydrocarbons can be achieved by reacting H_2 and CO over group VIII metals. A

wide variety of products, including alkanes, olefins, and oxygenated hydrocarbons, can be produced by this means. The distribution of products depends upon the nature of the catalyst and reaction conditions.

Many excellent reviews have been published discussing the thermodynamics, kinetics and reaction mechanisms pertaining to the Fischer-Tropsch reaction (1-4). This review of the literature will deal primarily with topics pertaining specifically to Ru.

2. Kinetic Studies over Ruthenium

Ruthenium has received the attention of researchers investigating Fischer-Tropsch chemistry for several reasons. Ruthenium provides the highest molecular weight distribution at 1 atm and at the same time exhibits the highest specific activity of the group VIII metals (5). Furthermore, Ru catalysts produce essentially straight chain hydrocarbons with only trace amounts of oxygenated products detected at elevated pressures (6,7).

The synthesis has been studied at atmospheric (5,8,9) and greater than atmospheric pressures (6,7,10). In general, the formation of higher molecular weight products is favored at lower temperatures, around 200°C, and higher pressures. The extent of reactant conversion has an effect on product distribution (6). In addition to the synthesis conditions, the effects of catalyst weight loading, metal particle size (7), and metal-support interaction (7,11) have also been investigated. King (7) reports that the specific

activity of Ru increases as the crystallite size increases and there appears not to be a support effect.

The kinetics of methane formation, as measured by several groups, can be correlated using equation (1)

$$N_{CH_4} = A\exp(-E/RT)P_{H_2}^{X} P_{CO}^{Y} \qquad (1)$$

where N_{CH_4} is the rate of methane production per surface site. Table 1 presents the results. The form of the rate expression appears unaffected by increases in pressure. For example, using Vannice's (5) parameters a pre-exponential, A, is calculated for King's (7) data at 4 atm. The calculated value, 3.05×10^5 sec^{-1} $torr^{x-y}$, is very close to that reported at 1 atm. In general there is an inverse order dependence on the partial pressure of CO showing that CO inhibits the reaction.

Ruthenium catalyst systems show a consistent deactivation pattern regardless of pressure. Dalla Betta et al. (9) and Everson et al. (6) have documented the change in activity with duration of the synthesis. The deactivation is affected by the H_2/CO ratio. Karn et al. (10) note that decreasing H_2/CO ratios lead to increased Ru deactivation over the course of the synthesis. Since the product distribution remained constant while the overall activity decreased, Everson et al. speculated that the deactivation was associated with a loss of active area. Several groups attribute this loss of area to a build-up of a carbonaceous residue on the Ru surface.

Table 1

Empirical Kinetic Expressions for the Hydrogenation of CO on Ru

Catalyst	Total Pressure (atm)	H_2/CO	T(°K)	A $sec^{-1}torr^{x-y}$	E Kcal/mole	X	Y
5% Ru/Al_2O_3 (5.12)	1	3	478-503	7.4×10^5	24.2±1.2	1.6±.1	-0.6±.1
1.5% Ru/Al_2O_3 (8)	0.75	3	513	3.1×10^5	24	1.8	-1.1
5% Ru/SiO_2 (11)	1	3	548	-	27	-	-
0.5% Ru/Al_2O_3 (10)	21.4	3	503-543	-	-	1.33	-0.3

3. Infrared and Adsorption Studies

A great deal of insight concerning the synthesis reaction can be gained from studies of individual gases with supported and unsupported Ru. These studies have utilized techniques such as infrared spectroscopy, AES, XPS, UPS, and Temperature Programmed Desorption to obtain information about adsorbate/surface interactions.

Infrared investigations of CO adsorbed on Ru have been reported for alumina- (18,19) and silica-supported (13-16,20) catalysts. The transmittance spectrum of CO adsorbed on Ru exhibits a broad band centered above 2000 cm^{-1}. The band is attributed to the C-O stretch of linearly adsorbed CO. While the spectrum typically exhibit a tail of the broad band extending well below 2000 cm^{-1}, there are no reports of a well resolved band which might be attributed to bridged bonding on supported surfaces. Table 2 summarizes the results of these investigations. The peak location is generally in the range of 2030 cm^{-1}.

In several of the cited studies other IR bands near 2100 cm^{-1} have been reported. These are assigned to CO adsorbed on oxidized and partially oxidized Ru surfaces. Since Fischer-Tropsch synthesis takes place under strongly reducing conditions, CO and H_2, bands present during the synthesis are expected to be those represented in Table 2.

Dalla Betta and Shelef (18) and King (19) have reported IR spectra taken under synthesis conditions for Ru/Al_2O_3 catalysts. In the presence of H_2 and CO at 523°K, Dalla

Table 2

CO Infrared Bands on Ruthenium

	ν_{CO} (cm^{-1})
4% Ru/SiO_2 (20)	2040
6% Ru/SiO_2 (14)	2030
2-6% Ru/SiO_2 (13)	2010-1990
5% Ru/Al_2O_3 (16)	2028
5% Ru/SiO_2 (16)	2043

Betta and Shelef observed a broad band centered at 2043 cm^{-1}. With increasing temperatures the IR band during the interaction of H_2 and CO is seen to shift from 1996 cm^{-1} at 523°K to 1925 cm^{-1} at 623°K. These studies indicated that even under reaction conditions CO is present as a linear structure.

Coadsorption studies of McKee (21) have shown that a Ru catalyst saturated with CO is capable of subsequent adsorption of nearly a monolayer of H_2. Based on this Dalla Betta and Shelef (18) have argued that the presence of adsorbed hydrogen may increase the availability of electrons for back-bonding from the metal to the adsorbed CO. This would explain the shift from 2043 to 1996 cm^{-1}, in accordance with the proposed model for CO adsorption discussed by Broden et al. (23). The shift with increasing temperature may in some way be related to the observed loss in activity reported by several groups. This loss has been attributed to a carbonaceous residue. While bulk carbides are not possible with Ru, carbon surface layers are. Carbides of W have been shown to have surface valence states which are "Pt-like" (24), that is there is an increase in the density of d-level electrons in the W-carbide over W. In a similar fashion the carbonaceous residue may increase the density of electrons at the surface, which would lead to more back donation and a lower C-O stretching frequency.

Desorption studies of CO from Ru have provided insight into the various adsorbed states of CO. While continually monitoring the gas phase over the surface, CO is desorbed by

rapidly increasing the temperature of the Ru. The temperature at which CO desorbs can be related to the activation energy for desorption, which is synonymous with the binding energy in the case of CO adsorption on Ru. This technique has been applied to CO adsorbed on supported Ru (22,25,26,27) and single crystal faces of Ru (28-31). Table 3 summarizes the binding energies reported for CO on Ru.

Single crystal studies show that at pressures below 10^{-5} torr, CO adsorbs molecularly on Ru with an initial binding energy near 29 Kcal. Increasing the coverage results in the appearance of a second adsorbed molecular state on a (001) surface with a binding energy of 25 Kcal. Increased exposure on a (110) surface leads to a shift in the original desorption peak, indicating a decreased binding energy from 26.9 to 22.8 Kcal. The lower binding energy appearing at higher coverages is associated with a CO-CO repulsive interaction. The application of LEED, XPS, UPS, AES, and work function measurements in conjunction with flash desorption confirms a molecularly bound state on the single crystal faces of Ru. In all these studies CO did not thermally dissociate.

The application of temperature programmed techniques to CO adsorbed on alumina-supported Ru at 1 atm indicates somewhat different behavior than CO adsorbed on single crystal faces of Ru at high vacuum. Low and Bell (25) have observed two desorption peaks for which they determine binding energies of 27 and 37 Kcal. Comparison of these binding energies with those reported for single crystal surfaces

Table 3

Activation Energies of CO

Desorption from Ruthenium

		E_d (Kcal)		
5% Ru/Al_2O_3	(25)		27	37
Ru(100)	(28)	24.4	30.1	
Ru(001)	(29)	23.5	28	
Ru(001)	(31)	25	29	34-37[a]
Ru(110)	(30)	22.8-26.9		

(a) After bombarding with 100 eV electrons

suggests that the low energy state, 27 Kcal, corresponds to molecularly adsorbed CO. The second state on supported Ru, 37 Kcal, may be related to the high temperature peak, referred to as β-CO, which Fuggle et al. (31) have observed following electron bombardment of CO adsorbed on a Ru (001) surface. While UPS, XPS, and XAES observations indicated that the appearance of β-CO was accompanied by CO dissociation and that β-CO occupied two surface sites, the exact structure of β-CO could not be established. Since the desorption activation energies associated with β-CO, 34-37 Kcal, are comparable, Low and Bell (25) speculated that β-CO may have formed on Ru/Al_2O_3 under the conditions of their study.

Low and Bell have also shown that at 1 atm upon heating CO adsorbed on 4 wt% Ru/Al_2O_3 above 415°K some CO dissociates, forming CO_2 and carbon. The studies of Kabo et al. (27) and McCarty et al. (26) confirm thermal dissociation of CO on alumina-supported Ru at 1 atm. In addition, Singh and Grenga (47) have reported carbon deposition on a polycrystalline Ru sphere exposed to 760 torr of CO at 823°K. These observations are in contrast to the high vacuum single crystal studies in which CO did not thermally dissociate. The presence of a high partial pressure of CO over the catalyst, which is absent in the vacuum studies, has been argued (25) to react with and remove surface oxygen, O_s, formed when CO dissociates. By removing surface oxygen, the equilibrium of the dissociation reaction,

$$CO_s + S \rightleftarrows C_s + O_s$$

is shifted to the right.

4. Mechanistic Interpretations

Two principle mechanisms for Fischer-Tropsch synthesis over group VIII metals have evolved. One school of thought holds to the view that CO dissociates before reacting with hydrogen to form hydrocarbons. This has been classified as the "carbide" mechanism. The second general scheme involves an oxygenated precursor. In such a scheme undissociated CO is partially hydrogenated before reacting further.

The carbide theory was first proposed by Fischer and Tropsch (4) who suggested that metallic carbides are formed as intermediate products, from dissociated CO, and that these carbides are reduced by the hydrogen present to form methylene groups. The methylene groups are either hydrogenated to form methane or polymerize into hydrocarbon chains which subsequently desorb. The mechanism can be represented by the following steps:

$$CO_{(g)} + M \rightarrow M\text{-}CO \qquad (1)$$

$$H_{2(g)} + 2M \rightarrow 2\ M\text{-}H \qquad (2)$$

$$M\text{-}CO + M \rightarrow M\text{-}C + M\text{-}O \qquad (3)$$

$$M\text{-}O + M\text{-}H \rightarrow M\text{-}OH \qquad (4)$$

$$M\text{-}OH + M\text{-}H \rightarrow H_2O_{(g)} + 2M \qquad (5)$$

$$M\text{-}C \xrightarrow{2M\text{-}H} M{=}CH_2 \xrightarrow{2\ M\text{-}H} CH_{4(g)} + 3M \qquad (6)$$

$$M{=}CH_2 + M{=}CH_2 \xrightarrow{M\text{-}H} M\text{-}CH_2\text{-}CH_3 + M \qquad (7)$$

$$M{=}CH_2 + M\text{-}CH_2\text{-}R \xrightarrow{M\text{-}H} \text{Paraffins, Olefins} \qquad (8)$$

$$M\text{-}CH_2\text{-}R + M\text{-}OH \xrightarrow{M\text{-}H} \text{Oxygenated hydrocarbons} \qquad (9)$$

The carbide theory as proposed by Fischer and Tropsch and expanded upon by Craxford and Rideal (40), while attractive, was not found to be consistent with experimental data (41,42,43). Studies in which Co and Fe were pre-carbided with ^{14}CO (43) and subsequently exposed to H_2 and CO failed to produce large quantities of ^{14}C labeled hydrocarbons. This result led to the conclusion that bulk or surface carbides played an unimportant role in Fischer-Tropsch synthesis. However, in one of these studies Kummer et al. (43) discussed the possibility that an "incipient surface carbide" could form on the surface during the synthesis and then undergo the hydrogenation and subsequent reaction according to the mechanism shown above. More recently evidence has been obtained that such a mechanism may be operative on the surface of Ru and other transition metal catalysts. A discussion of these results is given later.

Storch et al. (4) proposed a different mechanism involving the oxygenated intermediate, CHOH, an enol. This mechanism can be represented by the following steps:

$$CO_{(g)} + M \longrightarrow \begin{matrix} O \\ \| \\ C \\ \| \\ M \end{matrix} \qquad (10)$$

chain initiation:

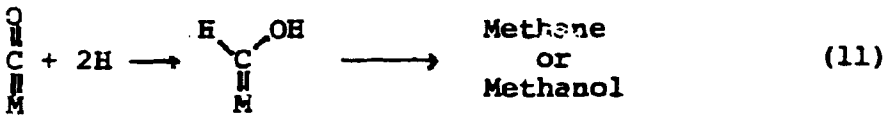

(11)

propagation:

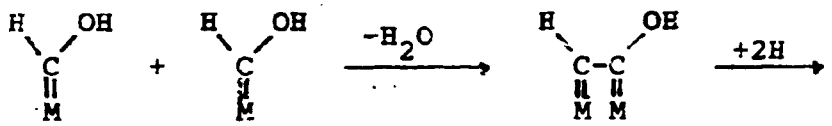

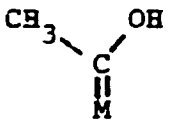

(12)

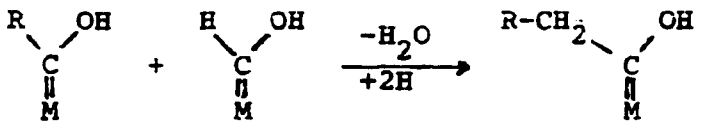

(13)

termination:

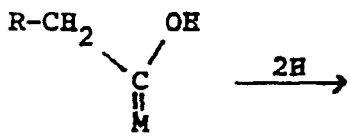

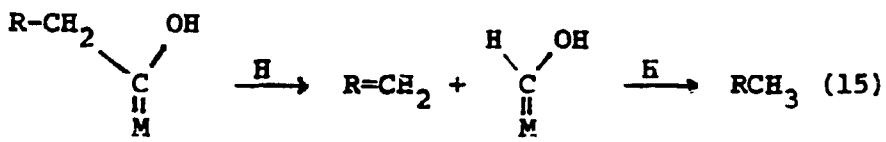

The enol can be hydrogenated to form either methane or methanol, reaction 11, or it can undergo a condensation reaction to form higher molecular weight hydrocarbons.

This mechanism is supported by alcohol incorporation into synthesis products (1,44,45), the one to one adsorption of H_2 and CO on several metals without product formation (21), and infrared observations over Fe (32,33). Using ^{14}C labeled alcohols Emmett and coworkers (44,45) arrived at the suggestion that either the alcohol or a surface complex formed by adsorption of the alcohol behaves like an intermediate in Fischer-Tropsch synthesis over Fe. They assumed the alcohol adsorption complex to take the form, MCRHOH, which differs from an enol, MCROH. A mechanistic scheme for alcohol incorporation was presented (45) which was compatible with enol structures. Blyholder (32,33) reported C-H and O-H infrared stretching frequencies at 180°C over Fe/SiO_2 under synthesis conditions. The O-H bands were shown to be present under reaction conditions and absent when exposing the catalyst to H_2/He and H_2O/He mixtures, indicating an adsorbed species giving rise to the O-H bands may be a reactive surface intermediate. Blyholder assigned the bands to the enol structure.

Many variations of the two general mechanisms discussed above have been published. The central question remains whether CO dissociates before reacting with hydrogen. In addition, if CO does dissociate, the dissociated carbon may only participate in chain initiation. This possibility is based on the work of Emmett and Blyholder (35,36). Through the use of labeled ketene, CH_2CO, they concluded that CH_2 groups may initiate chain growth but subsequent propagation

of a chain involves CO. However, the means by which CO added to the chains was not determined. Olivé and Olivé (34) have recently proposed a mechanism which takes Emmett's and Blyholder's observations into consideration. They propose that CO inserts into the growing carbon chain, is hydrogenated to an enol, loses water, and begins the sequence over again or is terminated. This mechanism is presented below.

(16)

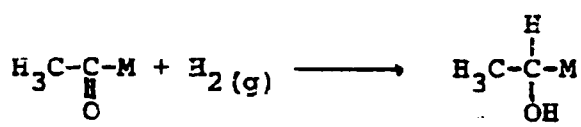

(17)

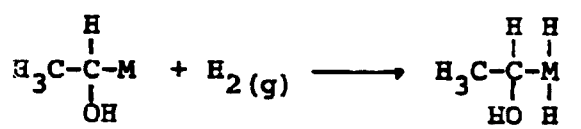

(18)

propagation:

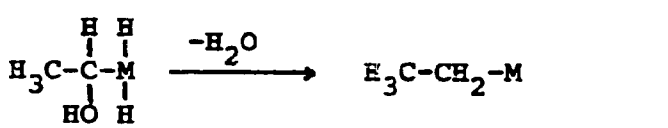

(19)

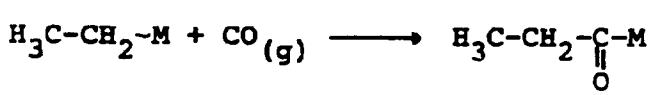

(20)

termination:

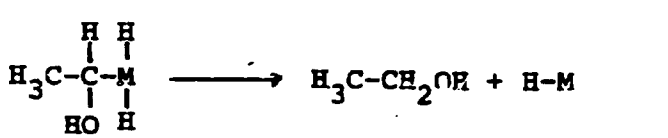

(21)

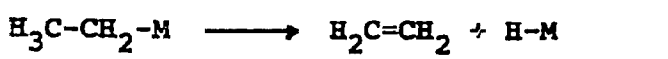

(22)

For the specific case of Fischer-Tropsch synthesis over Ru evidence has been presented in support of the three mechanisms discussed earlier. Several recent studies appear to favor the occurrence of the enol intermediate. Investigations of the adsorption behavior of CO and CO/H_2 mixtures have shown that at near monolayer coverage by CO, a monolayer of H_2 is adsorbed without the formation of synthesis products. McKee (21) explained the 1:1 adsorption by postulating the presence of an adsorption complex, HCOH. Goodman et al. (30) have observed an interaction between adsorbed hydrogen and carbon monoxide without methane formation. They found the desorption energy of hydrogen increased in the presence of CO. In both cases there appeared to be an interaction between H_2 and CO without product formation leading to the suspicion that a complex of the form, HCOH, was present. Other evidence in support of the enol mechanism over Ru has come through interpretation of kinetic data (5).

As previously discussed, the application of temperature programmed techniques to CO adsorbed on supported Ru has shown that CO will thermally disproportionate according to reaction 23 (22, 25, 26, 27).

$$M\text{-}CO + M\text{-}CO \longrightarrow M\text{-}C + M + CO_2 \qquad (23)$$

The carbon formed by the disproportionation is very reactive toward hydrogen, producing CH_4, C_2H_6 (25, 27) and C_3H_8 (27) at room temperature. Adsorbed CO does not react with

hydrogen at room temperature. These results have renewed interest in mechanisms involving a non-oxygenated intermediate.

Support for CO insertion into the growing chain has come from the interpretation of kinetic data. Dautzenberg et al. (46) carried out a series of experiments in which a Ru catalyst alternately was exposed to a H_2/CO synthesis mixture and a H_2/He mixture. The transient response of the Fischer-Tropsch products to varying exposure times was investigated and found to satisfy Schulz-Flory polymerization kinetics. The insertion of CO, acting as the monomer for chain growth, was postulated to satisfy the transient data.

II. EXPERIMENTAL METHODS

A. Experimental Apparatus

The apparatus used for the present studies was designed to permit in situ infrared spectra to be taken at the same time that kinetic measurements were obtained. Figure 1 is a schematic of the entire system. Relevant information for each component of the apparatus is discussed below.

1. Reactor

The reactor designed specifically for these experiments is shown schematically in Figure 2 and a photograph of the disassembled reactor is shown in Figure 3. The reactor is designed to fit within the sample compartment of a Perkin Elmer 467 infrared spectrometer. The entire reactor is made of type 304 or 316 stainless steel. The rectangular inner chamber (84.2 mm long, 12.7 mm wide, 38.1 mm high) of the reactor is coated with aluminum to reduce the catalytic activity of the stainless steel walls. The aluminum coating is oxidized at 430°C for two days to develop an impervious oxidized layer. This inner rectangular chamber is the reaction zone where the catalyst is positioned.

The catalyst is pressed into a self-supporting disk, 29 mm in diameter, and is positioned in the sample beam of the spectrometer. It is loosely held in an aluminum assembly shown in Figure 4. The second disk is pressed from Cab-O-Sil and is positioned in the reference beam to suppress the catalyst support spectrum. Because the gas path is the same for both beams, gas phase infrared absorbance is not detected.

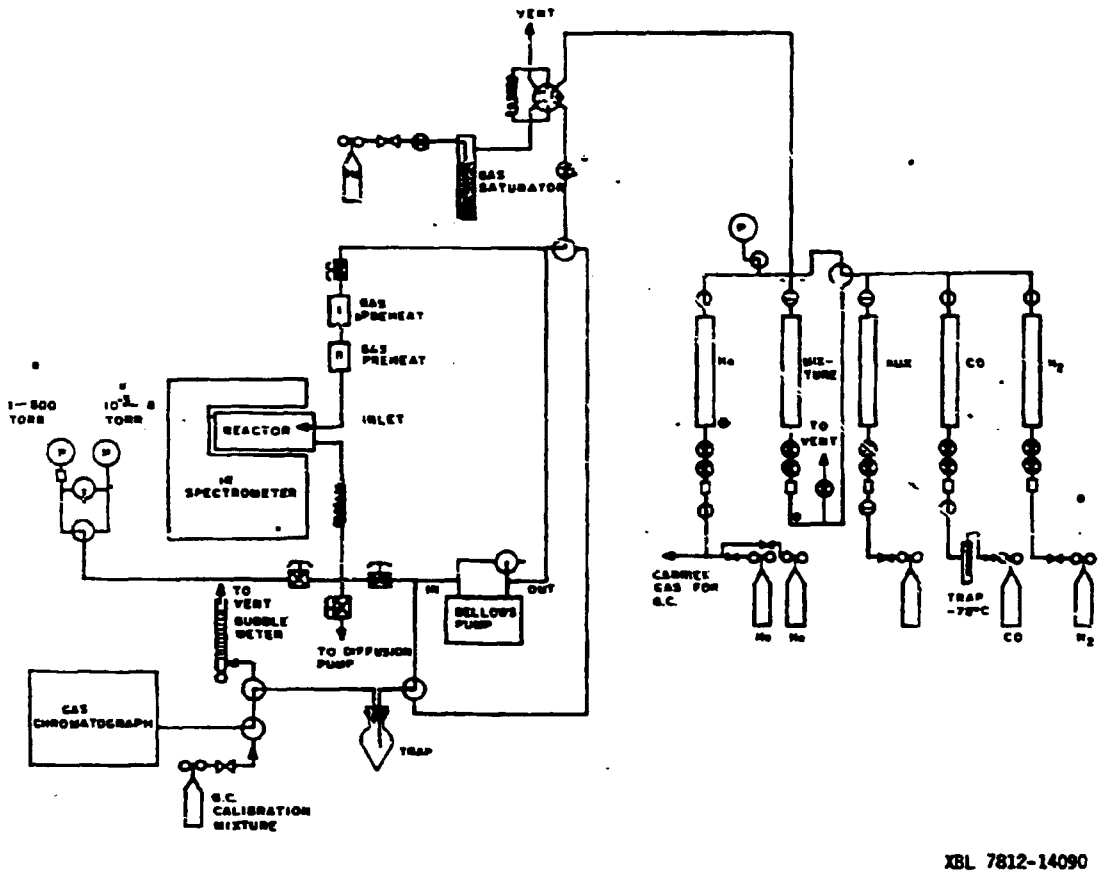

Figure 1. System schematic

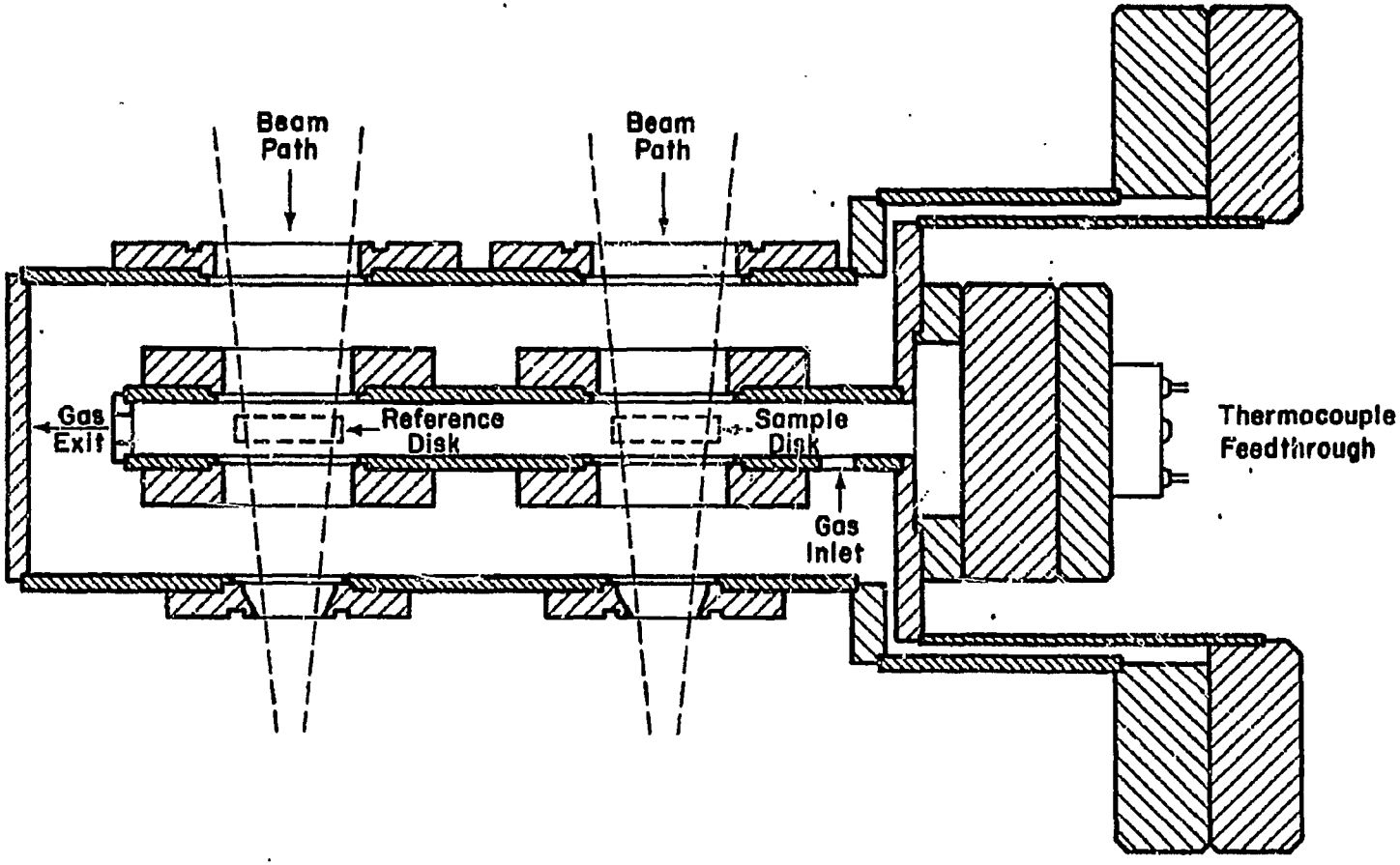

Figure 2. Reactor cross-sectional view

XBL 784-8314

Figure 3. Disassembled reactor

CB 773-1627

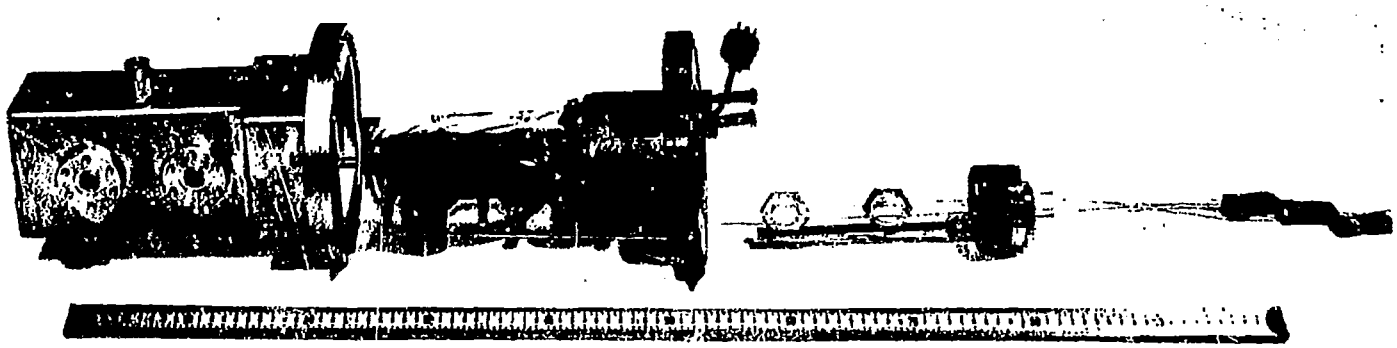

CBB 773-1627

Figure 3

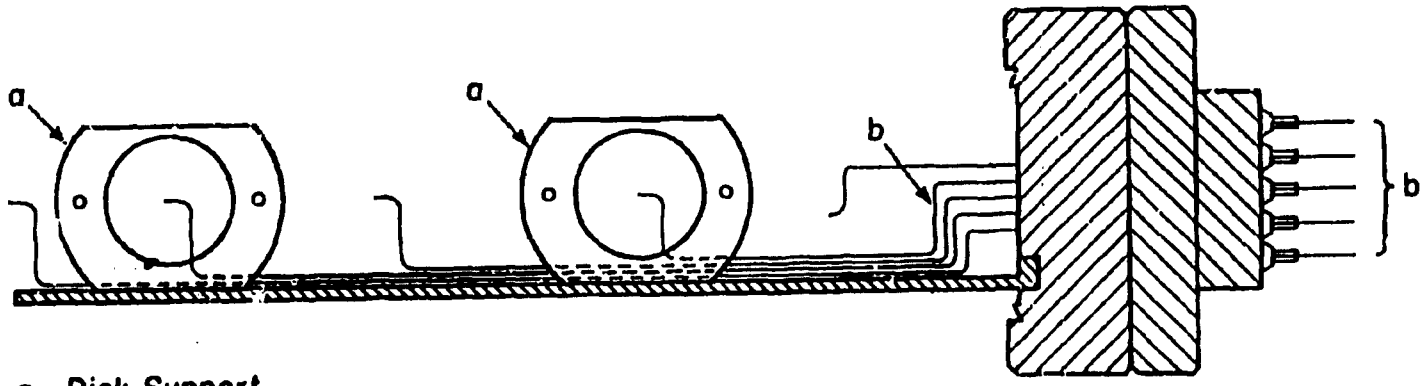

a. Disk Support
b. Stainless Steel Sheathed Thermocouple

XBL 7812-14089

Figure 4. Catalyst support assembly

Strip heaters placed on the top and bottom of the inner chamber allow it to be heated. Four temperatures are measured within the inner chamber. Stainless steel sheathed thermocouples are positioned adjacent to the disks to enable the catalyst and support temperatures to be measured. In addition, sheathed thermocouples are used to monitor the inlet and exit gas temperature. The thermocouple feed-through flange assembly, Fig. 4, is wrapped with heating tape to attain isothermal operation of the inner chamber. To minimize heat losses a vacuum, typically 10^{-2} torr, is maintained in the outer chamber. This limits heat losses to radiative transport.

The infrared optics consist of 2 sets of KBr and ZnSe circular windows. The infrared beam passages through the outer chamber are covered by KBr windows. The seal is made using Viton O-rings. The infrared passages through the inner chamber are covered by 2 mm thick ZnSe windows sealed to knife-edge flanges with Vac-Seal (Space Environment Laboratories, Inc.). An antireflection coating was applied to the ZnSe windows by the manufacturer, Eastman Kodak, to minimize reflective losses in the region of 3800-3000 cm^{-1}. The window combination allows spectra to be recorded over the range of 4000 to 650 cm^{-1}. Over this range approximately 50% of the source energy is lost in the infrared windows. The use of ZnSe limited the upper temperature of the reactor to 300°C.

The reactor could be operated from 10^{-7} torr to one atmosphere. Three sensors are used to monitor the pressure over the anticipated range. Figure 1 shows the location of a Wallace and Tiernan absolute meter covering the range 0-800 torr, a Baratron capacitance manometer covering the range 10^{-3}-8 torr, and an ionization gauge on the diffusion pump for pressures below 10^{-3} torr.

2. Gas Blending and Flow Systems

The reactor is operated in an open loop recycle mode. The gases are fed and removed from the recycle loop at a flow rate of 210 cm^3/min. A stainless steel metal bellows pump recirculates gas at 40 liters/min. This results in a recycle ratio of 190:1. Under these conditions the reactor can be treated as a CSTR (37). Gases exiting a CSTR are identical in composition to the gases within the reactor and hence over the catalyst.

As shown in Figure 1 the recycle loop contains the reactor, bellows pump and gas preheaters. The reactant gases are heated on each pass in Al tubing wrapped around copper blocks and are cooled in a 6 ft coiled section of Al tubing. Except for short lengths of stainless steel tubing needed at the inlet and outlet of the reactor, all hot surfaces are made of, or coated with, aluminum. This was done to minimize any catalytic activity of the Fe or Ni in stainless steel. These hot surfaces have approximately 2% of the activity of a catalyst disk.

Gases continually circulate within the recycle loop at 40 liters/min. The volume of this loop is 370 cm^3. This was determined by monitoring the dynamics after introducing a step change to the reactor. At the synthesis feed rate of 210 cm^3/min the reactor has a time constant of 1.76 min.

The feed mixture was blended using a bubble meter to set the flow of each reactant. While the manifold was provided with rotameters for each gas these were not used. Because of the low flow rates required for CO and H_2 (10 to 150 cm^3/min), it was found that the sapphire float for CO and H_2 stuck to the inner wall of the rotameter tube. All attempts to obtain reproducible and reliable rotameter performance failed.

3. Gas Analysis

A gas chromatograph, equipped with a thermal conductivity detector, is used to analyze the composition of the gases exiting the recycle loop. For most experiments, the water produced during the reaction:

$$H_2 + CO \rightarrow H_2O + \text{Hydrocarbons}$$

was trapped in dry ice to avoid saturating the chromatographic column. All gases exiting the recycle loop pass through a 6-way sampling valve before being vented. The valve is equipped with a 1 cm^3 sample loop.

The gases were only analyzed through C_3's. To achieve a separation of light reactants, H_2 and CO, from the products, CH_4, C_2H_4, C_2H_6, C_3H_6, C_3H_8, and CO_2, a 124 cm by

0.48 cm OD column of Porapak Q was used. The colum was operated isothermally at 120°C. Using a carrier (He) flow of 60 cm^3/min the last gas, C_3H_8, elutes from the column in 11.5 min.

A Matheson certified standard gas mixture was used each day to calibrate the GC. The mixture consisted of gases at concentrations close to those anticipated in the experiments. The molar concentration of a given component is based on peak height of the GC trace and is determined according to equation 2.

$$(\text{conc})_i = (\text{peak ht x attenuation})_i \frac{\text{concentration}}{\text{peak ht x attenuation}}_{\text{std}} \quad (2)$$

This procedure is based on the linearity of a calibration made with two different gas mixtures extrapolated to zero concentration.

B. Experimental Procedures

Prior to a kinetic run, the reactant gases were blended to give the proper partial pressure of CO and H_2. Helium was used as an inert to bring the total inlet flow to the reactor to 210 cm^3/min. This flow was held constant for all the experiments. In most experiments the recycle loop contained about 2-6% H_2 in He while the flows were being adjusted. This was done to ensure any oxygen entering in air leaks would be reduced with H_2 and not oxidize the Ru metal. Only when it was necessary to introduce a reactant mixture to a H_2 free system was the loop purged of H_2.

While the flows were being adjusted the GC was calibrated with the standard mixture. Temperatures were adjusted, using Variacs, to the synthesis temperature. After the catalyst and reference disk were at the desired temperature, a background spectrum over the range of 4000 to 1400 cm^{-1} was recorded.

A synthesis experiment was initiated by the introduction of the reactant feed stream into the recycle loop. Ten minutes (5.7τ, τ=1.76 min) after admitting the reactant mixture it is safe to assume the desired partial pressures are present over the catalyst and that the system is operating at steady state. Initial rate measurements were taken 10 min after admitting the reactants.

Infrared spectra were recorded over the range of 3800-1400 cm^{-1}. The interval between recording spectra and the range scanned was varied to suit the intention of the experiment. After the catalyst was regenerated, the spectrum 4000-1400 cm^{-1} was recorded and used to compare against those recorded during the synthesis and that recorded prior to admitting the reactants.

The synthesis was carried out for varying periods of time. Most synthesis experiments were 2 hours long. The common variable in all experiments is the initial gas sampling at 10 min. All rate data are based on this measurement.

After following the synthesis of hydrocarbons for a predetermined time, the flow of CO was stopped. Hydrogen

and He continued to flow. Initially the H_2/He flows were maintained at the levels present during the synthesis. It was determined that the total flow rate, Q_{tot}, and the partial pressure of H_2 had a strong influence on the reactivation of the catalyst. To isolate behavior resulting from the synthesis, a set of reactivation flows for H_2 and He was selected. After the flow of CO was stopped, H_2 and He were adjusted to the desired flows.

During reactivation the gas composition exiting the reactor and the infrared absorbance of CO and other adsorbed hydrocarbons was monitored as a function of time. The gas composition usually was analyzed until hydrocarbons produced during the reactivation could no longer be detected.

C. Catalyst Preparation

A Ru catalyst was supported on Cab-O-Sil, HS-5, which has a BET surface area of 325 +_ 25 m^2/gm and is in the form of 70 A° particles. The catalyst was prepared by precipitation of $RuCl_3$ from an aqueous solution of $RuCl_3 \cdot 3H_2O$ and distilled water. The support is contacted with the minimum amount of solution needed, 2 gm solution to 1 gm Cab-O-Sil, to wet it. The paste, formed in this fashion, is frozen by pouring liquid nitrogen on it. The frozen mixture is then placed under mechanical pump vacuum and maintained at dry ice temperature for several days. To prevent the migration of $RuCl_3$ within the paste, the paste was kept below the melting point of the solution while water was removed by sublimation. Freezing at liquid nitrogen temperature

results in a looser catalyst powder, which minimizes grinding and sieving time.

After the water has been removed by sublimation, the catalyst is ready to be reduced. The $RuCl_3$ is reduced directly to Ru under H_2 without calcining. The catalyst is placed in allundum extraction thimbles supported in a quartz tube. A Lindburg furnace is used to achieve reduction temperature. The reduction cycle consists of: flushing with He at 100 cm^3/min for 30 min at room temperature, followed by flushing with H_2 at 100 cm^3/min for 30 min at room temperature, and finally admitting a 50:50 mixture of H_2:He at 200 cm^3/min for the high temperature reduction. Under H_2/He, the temperature is raised over a 60 min period from room temperature to 400°C. The temperature is maintained at 400 °C for 120 min. After 120 min at 400°C, the furnace door is opened and the quartz tube is removed to quench the reduction. The H_2/He mixture continues to flow for 60 min to ensure the catalyst is cool before exposing it to the atmosphere.

The catalyst powder is crushed and sieved to sub 325 Tyler mesh, 45 μm. The catalyst is stored in a desicator to minimize contamination.

A self-supporting wafer is pressed from the treated powder. Approximately 200 mg is placed in a 1-1/8 in die made from tool steel. A force of 9480 lb/in^2 is applied to the face of the 1-1/8 in die for 7-8 min. The resulting disk is used for the kinetic and infrared studies.

Prior to using a disk for kinetic measurements, it is reduced in situ. The reactor is evacuated at 10^{-6} torr for 3 hrs at room temperature. After this it is heated to 275°C under flowing H_2/He for several days. The catalyst disk is exposed to a 6% H_2 in He mixture at temperatures greater than 191°C between experiments.

D. Catalyst Characterization

The catalyst was characterized by a variety of techniques. Ruthenium surface area was determined by H_2 chemisorption and direct crystallite size measurement by transmission electron microscopy. A semiquantitative analysis for trace metal impurities was done using emission spectrographic techniques. The actual weight loading, 4.73 wt% Ru, was determined analytically by spectrophotometric analysis of a prepared solution with NaSCN. The prepared solution is made by fusing the catalyst with NaOH and $KClO_3$, treating the resulting solution with HCl, and adding HF and H_2SO_4 to remove the SiO_2.

The difficulty of performing hydrogen chemisorption on supported Ru has been well documented (38,39). A procedure was chosen to minimize the time needed to achieve equilibrium uptake. A sample was sent to Pacific Sorption Service to determine BET surface area and Ru surface area by H_2 chemisorption. The catalyst has a BET surface area of 310 m^2/gm. The hydrogen adsorption was performed at 100°C, to speed up the uptake, at a partial pressure of 400 torr. The amount of H_2 adsorbed was 22 μmoles/gm of catalyst.

Assuming 1 atom of hydrogen per surface Ru metal atom (38) this corresponds to a dispersion of 0.094 surface Ru atoms/ total Ru atoms.

The uptake measurement can be used to calculate a metal particle size. The crystallites are assumed to be cubic. As derived in Appendix I.

$$L = \frac{5}{D \times (8.17 \text{Å}^2/\text{surface Ru})(7.27 \times 10^{-2} \text{molecules Ru}/\text{Å}^3)} \quad (3)$$

where: L is the edge of the cube in Å

D = surface Ru/total Ru

For a dispersion of 0.094 equation 3 predicts a particle size of 89.6 Å.

Particle size was also determined by transmission electron microscopy. The instrument (Phillips 301) used has a resolution of approximately 5 Å at 100 KV. The samples were prepared by dropping a water suspension of the catalyst powder onto a Formvar coated copper grid. In most of the specimens the catalyst migrated off the grid before the water evaporated. Because of this, only a limited number of crystallites, 89, could be found. This low number introduces considerable spread in the reported crystallite size.

Figure 5 is a micrograph of the catalyst powder. The Ru crystallites show up as dark spots against a grayish background of silica particles. By measuring the size of the Ru crystallites a mean crystallite diameter of 51 Å is determined.

Figure 5. Electron micrograph of Ru supported on Cab-O-Sil: magnification factor of 250 K

XBB 780-15853

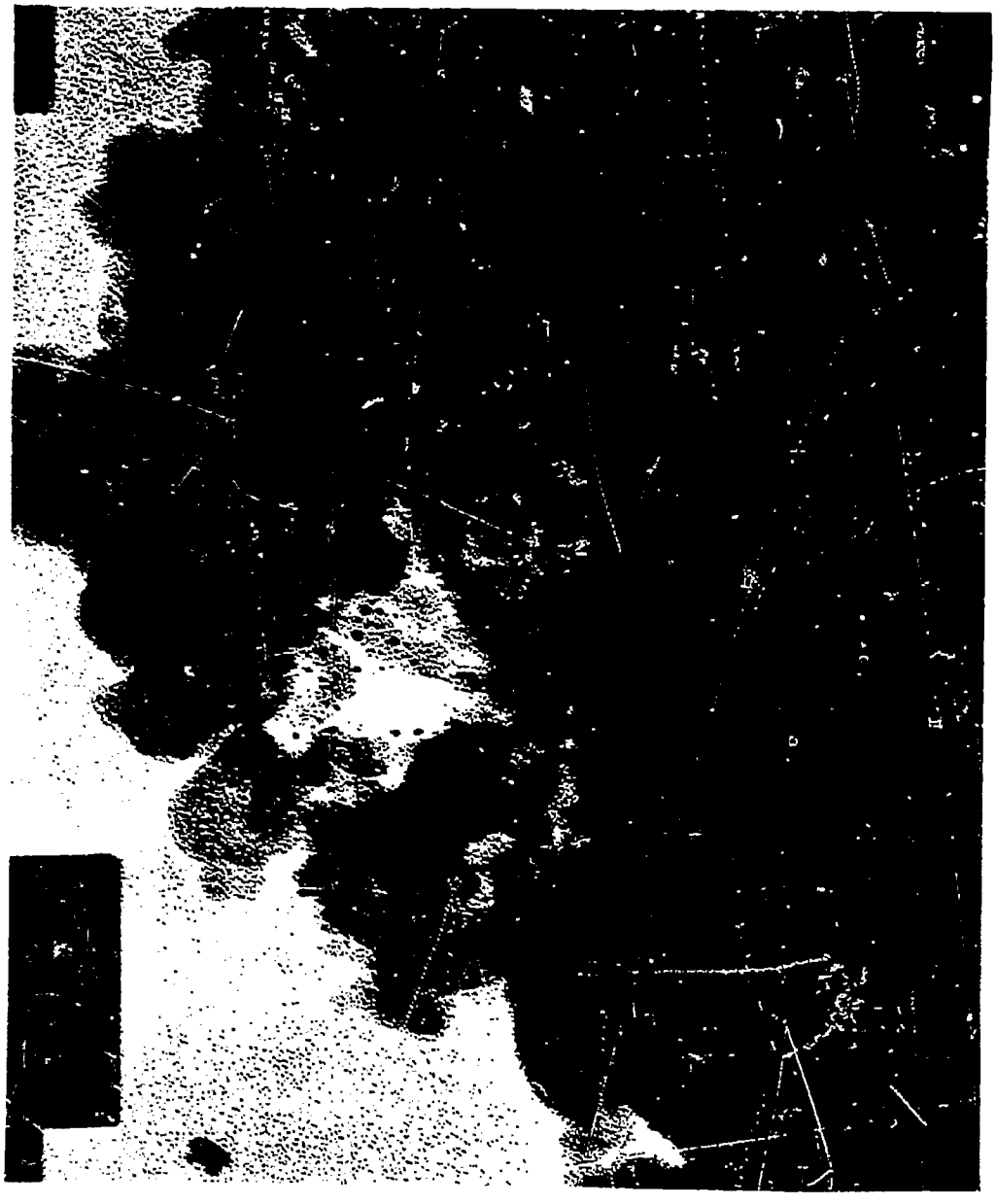

XBB 780-15853

Figure 5.

There is a discrepancy between the size predicted by H_2 chemisorption, 90 Å, and that measured by transmission electron microscopy, 51 Å. Several errors are associated with both methods. The microscopy results are based on 89 crystallites. A representative sample is usually closer to 500 crystallites. The size predicted by H_2 chemisorption is based on a 1:1 H:Ru ratio and the assumption that all surface sites are covered at 100°C in the 2 hr exposure period. While the discrepancy exists the results do show that the dispersion is poor and the mean crystallite size is at least 50 Å or larger. All specific rates, molecules of CH_4/site-sec, are based on the H_2 chemisorption measurements. If these measurements are in error the reported rates will be off by a constant amount.

The catalyst and support was analyzed by American Spectrographic Laboratories, Inc. for trace metal impurities. Table 4 presents the results. These results show that Ru is present in concentrations at least 400 times greater than any impurity, reported as an oxide, and that Ru is present in the same concentration as that determined quantitatively.

E. Materials

Hydrogen and helium were supplied by LBL and have a minimum purity of 99.999 and 99.998 mole% respectively. These gases were used as supplied without further purification. It was felt water removal would be senseless in that water is produced in the synthesis reaction. The CO, Matheson Ultra Pure 99.8 mole%, was passed through a packed

Table 4

Analysis for Trace Metal Impurities

	Cab-O-Sil	Catalyst
Ru[b]	-	4. %
B	0.01 % [a]	-
Mn	-	-
Ti	0.003	0.002
Al	0.001	<0.001
Mg	0.005	0.001
Ca	<0.001	0.001
Cu	<0.001	0.001
Fe	-	0.01
Cr	-	0.001
Ni	-	0.001

(a) reported as oxides of the elements

(b) reported as metal

tube at -78°C. This was done to remove any Fe or Ni carbonyls which may form in the cylinder.

III. REACTION RATE MEASUREMENTS AND INFRARED SPECTRA OF ADSORBED SPECIES

The results of the kinetic studies and the infrared spectra of adsorbed species are presented in this chapter. The results are discussed and a mechanism for methane formation is developed. The results suggest a possible scheme for synthesis of other hydrocarbons and this is also discussed.

A. Results

1. Kinetic Measurements

Preceeding each measurement of reaction kinetics the catalyst was reduced overnight in flowing H_2 at the intended reaction temperature. Following the introduction of the reaction mixture the gas composition was analyzed as a function of time. Figure 6 illustrates an example of the data. The points show that the rate of methane formation, relative to the initial rate measured at 10 min. declines as a function of time, indicating a loss in catalyst activity. The rate of deactivation is seen to increase as the ratio of H_2 to CO over the catalyst is decreased. For a fixed H_2/CO ratio the deactivation rate is also observed to increase with CO partial pressure as shown in Fig. 7. The catalyst deactivation is reversible, however, and the original activity can be restored by heating the catalyst overnight in flowing H_2 at temperatures between 190 and 275°C.

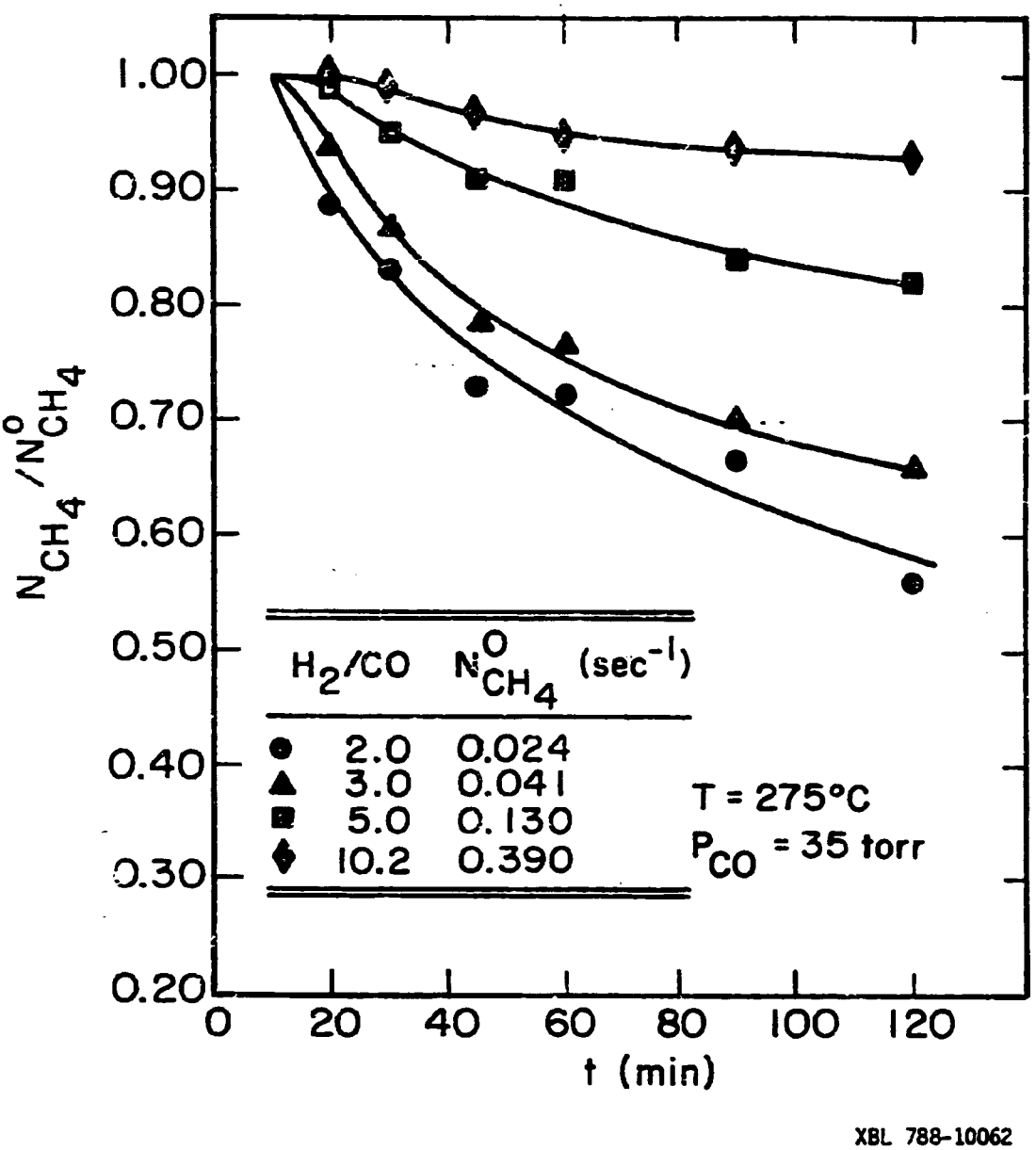

Figure 6. Effect H_2/CO ratio at fixed CO partial pressure on the rate of methane formation and catalyst deactivation

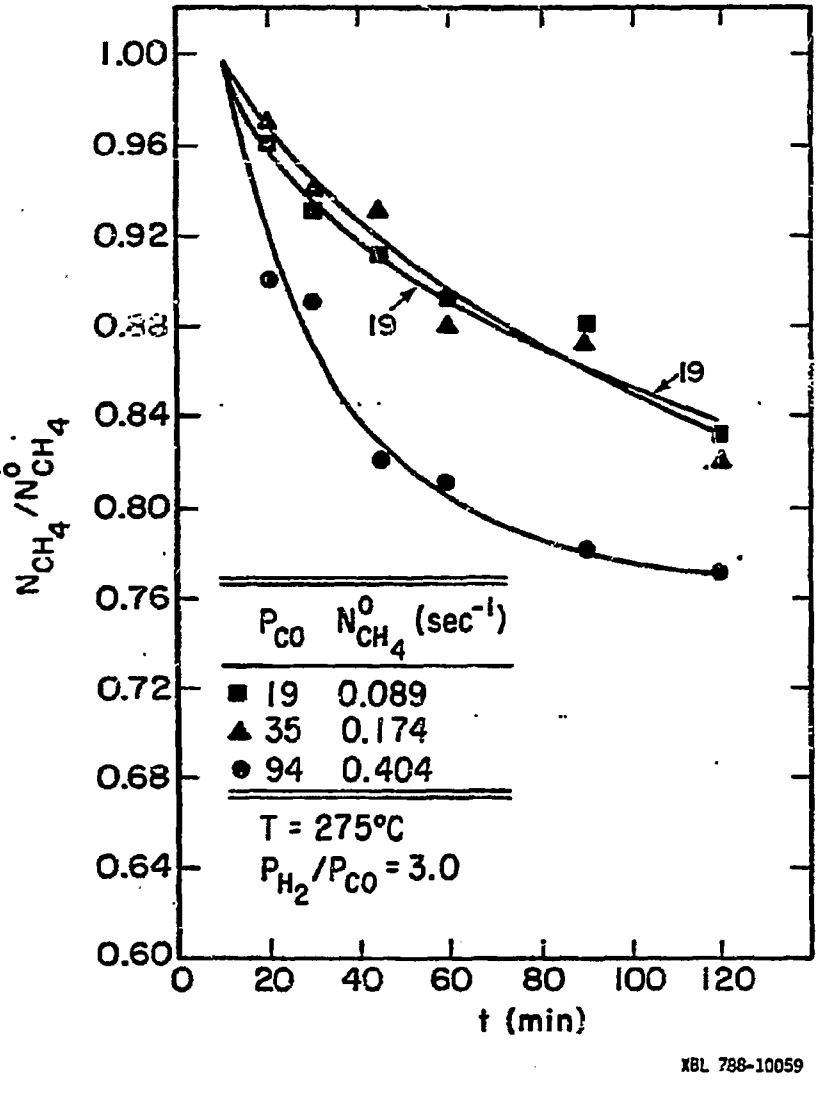

Figure 7. Effect of CO partial pressure at fixed H_2/CO ratio on the rate of methane formation and catalyst deactivation

To minimize the influence of deactivation on the measured kinetics, only the initial rates, measured at 10 min., were used. Data were taken at CO partial pressures between 16 and 200 torr, H_2/CO ratios between 1 and 20, and temperatures between 191 and 275°C. The CO conversion observed ranged from 0.1% for the lowest reaction rates to 40% for the highest rates. As exemplified by the data shown in the legends of Figs. 6 and 7, the rate of methane formation was observed to increase with H_2/CO ratio at a constant CO partial pressure and to increase with CO partial pressure at a constant H_2/CO ratio.

The dependence of the rate of methane formation on the partial pressures of H_2 and CO was determined by a nonlinear least square fit of the accumulated rate data to the following empirical expression

$$N_{CH_4} = Ae^{-E/RT}P_{H_2}{}^{X}P_{CO}{}^{Y} \qquad (4)$$

where N_{CH_4} is the rate of methane production per surface Ru site, where A is the pre-exponential factor, E the apparent activation energy, and X and Y are exponents on the partial pressures of H_2 and CO respectively. The quality of the fit between the data and eqn. 4 is shown in Fig. 8. Over three orders of magnitude in N_{CH_4}, the average absolute relative deviation between the calculated and observed turnover numbers is $\pm$ 15%.

In addition to methane, the products were found to contain ethane, propylene, and propane. Ethylene, when

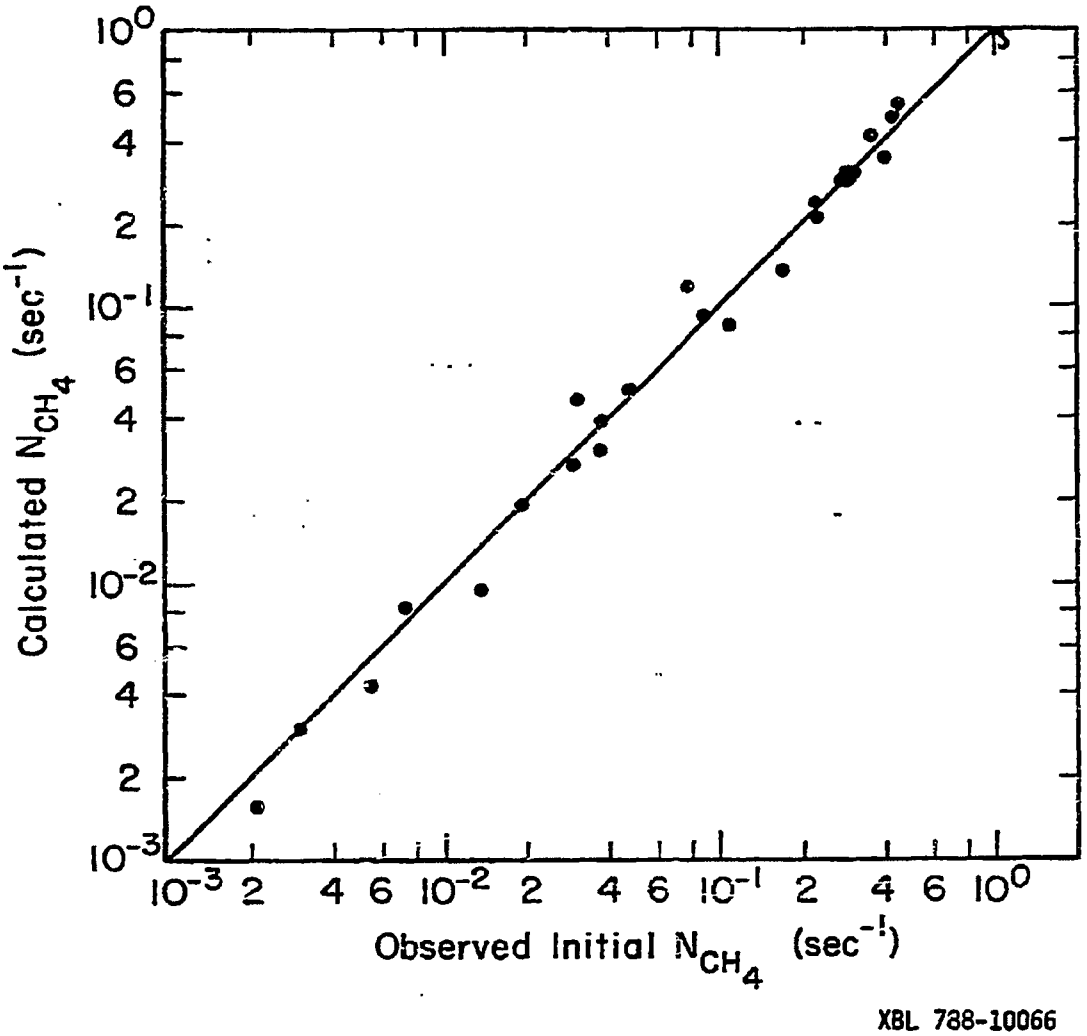

Figure 8. Comparison of calculated and experimental rate of methane synthesis

detected, was present only in trace quantities and its concentration could not be determined accuately. The yields of higher molecular weight products were independent of catalyst deactivation, indicating that overall activity as well as methanation activity decays with time. The dependence of product distribution on reaction conditions is shown in Figs. 9 through 11. It is apparent that the formation of high relative yields of C_2 and C_3 products is favored as the temperature and the H_2/CO ratio decrease and as the partial pressure of CO increases. A particularly interesting product composition was obtained when the temperature was set to 191°C, the CO partial pressure to 195 torr, and the H_2/CO ratio to 2. Under these conditions only propylene was observed in addition to methane and the propylene to methane ratio was essentially one to one.

The only nonhydrocarbon product observed in significant concentrations was water. Carbon dioxide was detected, but its concentration was negligible compared to that of water. These results indicate that the reaction products are far from equilibrium with respect to the water gas shift reaction.

2. In Situ Infrared Spectroscopy

Figure 12 shows typical infrared spectra recorded under reaction conditions at 191, 225 and 275°C. At all three temperatures the most prominent feature is a strong band at 2030 cm^{-1}, characteristic of CO linearly adsorbed on a fully reduced silica-supported Ru catalyst (14,20). The position of the CO band remained constant to within $\pm$ 5 cm^{-1}

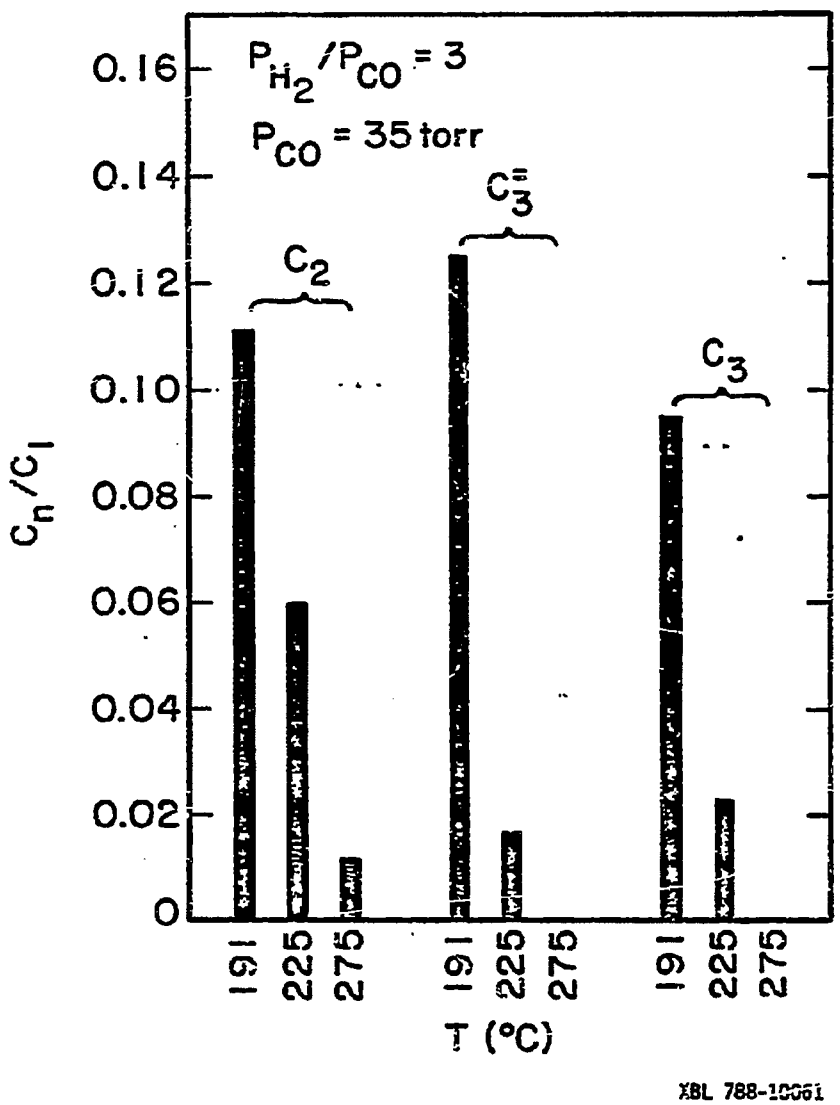

Figure 9. Dependence of product selectivity on temperature

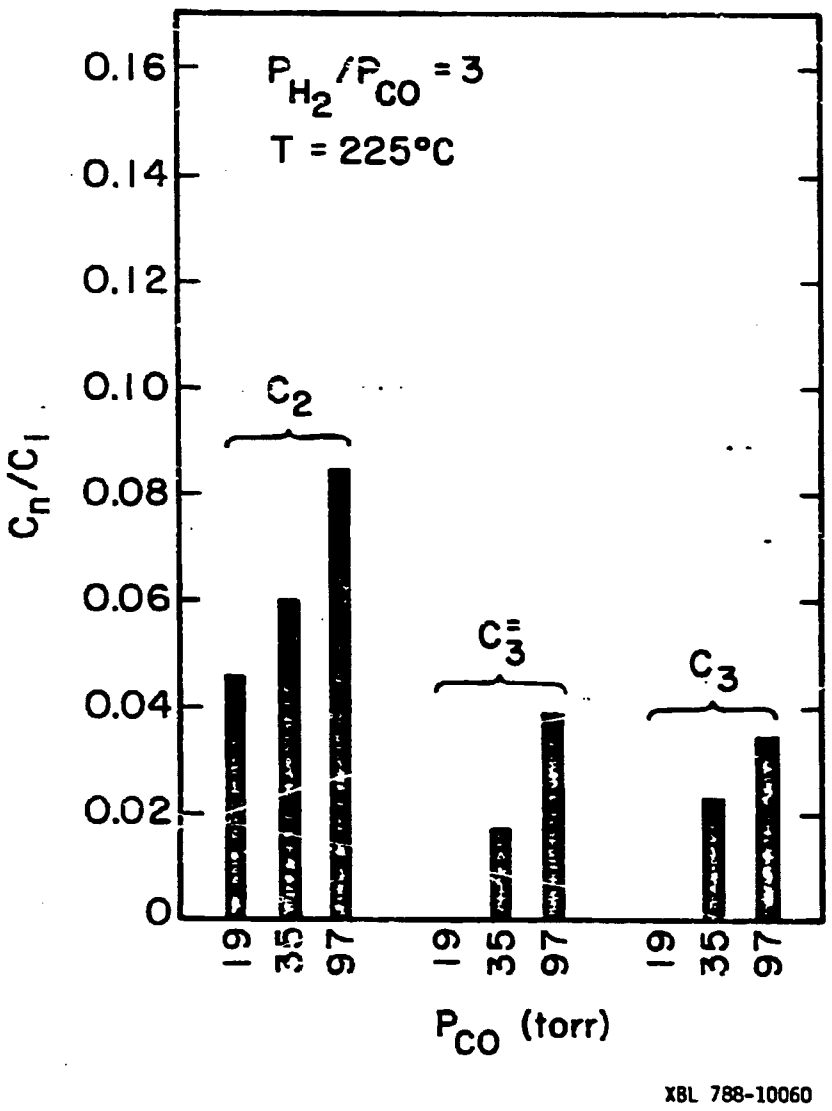

Figure 10. Dependence of product selectivity on CO partial pressure

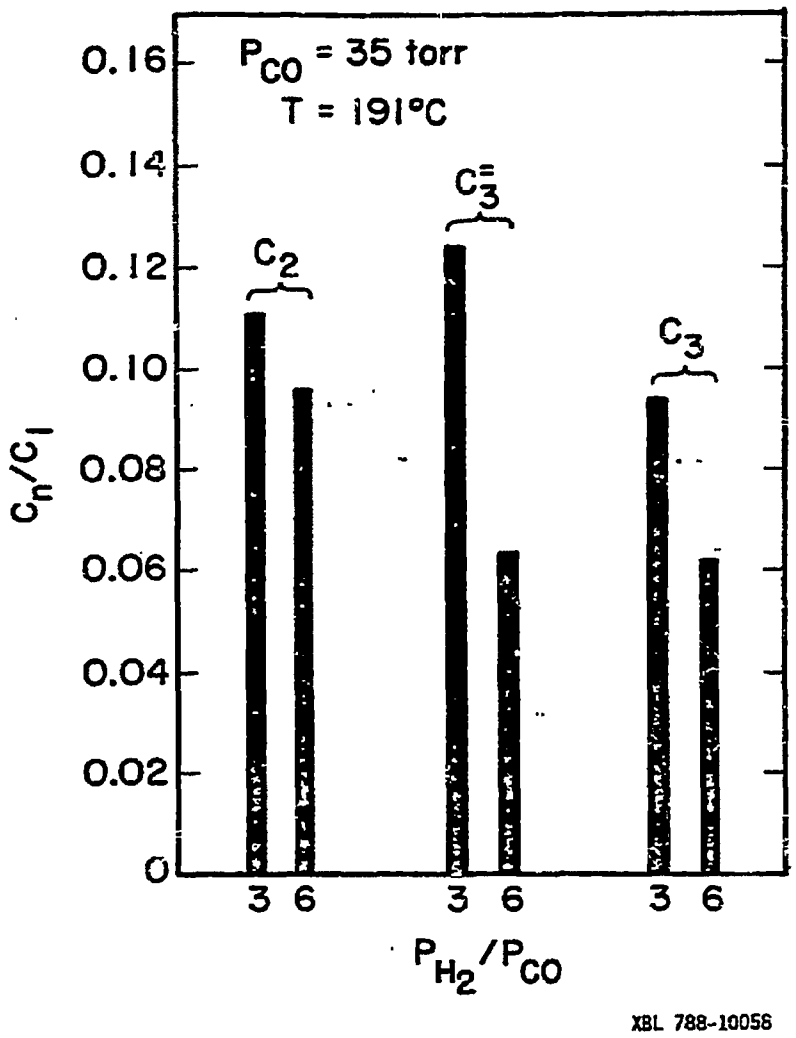

Figure 11. Dependence of product selectivity on H_2/CO ratio

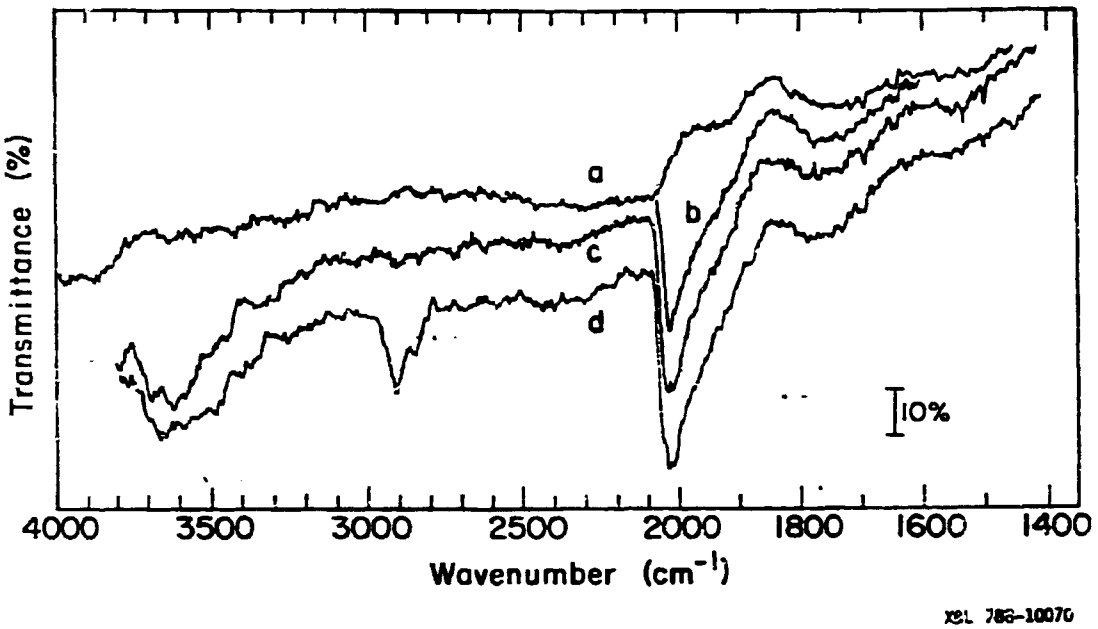

Figure 12. Infrared Spectra taken under reaction conditions: a) background at T = 275°C; b) during reaction of T = 275°C, P_{CO} = 99 torr, P_{H_2}/P_{CO} = 3; c) during reaction at T = 225°C, P_{CO} = 102 torr, P_{H_2}/P_{CO} = 3; d) during reaction at T = 191°C, P_{CO} = 197 torr, P_{H_2}/P_{CO} = 2.

for all of the reaction conditions used in this work and did not change as the catalyst deactivated. The dependence of the CO band absorbance on reaction conditions is shown in Fig. 13. The data points show that at a fixed temperature the absorbance is essentially independent of either the CO partial pressure or the H_2/CO ratio. Whatever variations are observed are well within the scatter of the data. While not noted in Fig. 13, it was found that the band intensity was also independent of the extent of catalyst deactivation. To further test whether the presence of H_2 affects the intensity of the CO band, the catalyst was contacted with CO/He mixtures in which the CO partial pressures were similar to those used under reaction conditions. The resulting spectra showed a CO band centered at 2030 cm^{-1}, identical in shape to that shown in Fig. 12. At each temperature, the CO band absorbance was essentially the same as that given by the horizontal lines shown in Fig. 13. The only variable found to influence the CO band intensity was temperature. Both in the absence and presence of H_2 the band intensity was observed to decrease with increasing temperature.

Spectrum d in Fig. 12 shows three bands at 2950, 2910 and 2845 cm^{-1} in addition to the CO band at 2030 cm^{-1}. These new features are observed at 191°C when the CO partial pressure is above 180 torr and the H_2/CO ratio is below 2. The bands increase in intensity very slowly and become prominent only after 20 min. Based upon the positions of the bands, the weak shoulder appearing at 2950 cm^{-1} can be

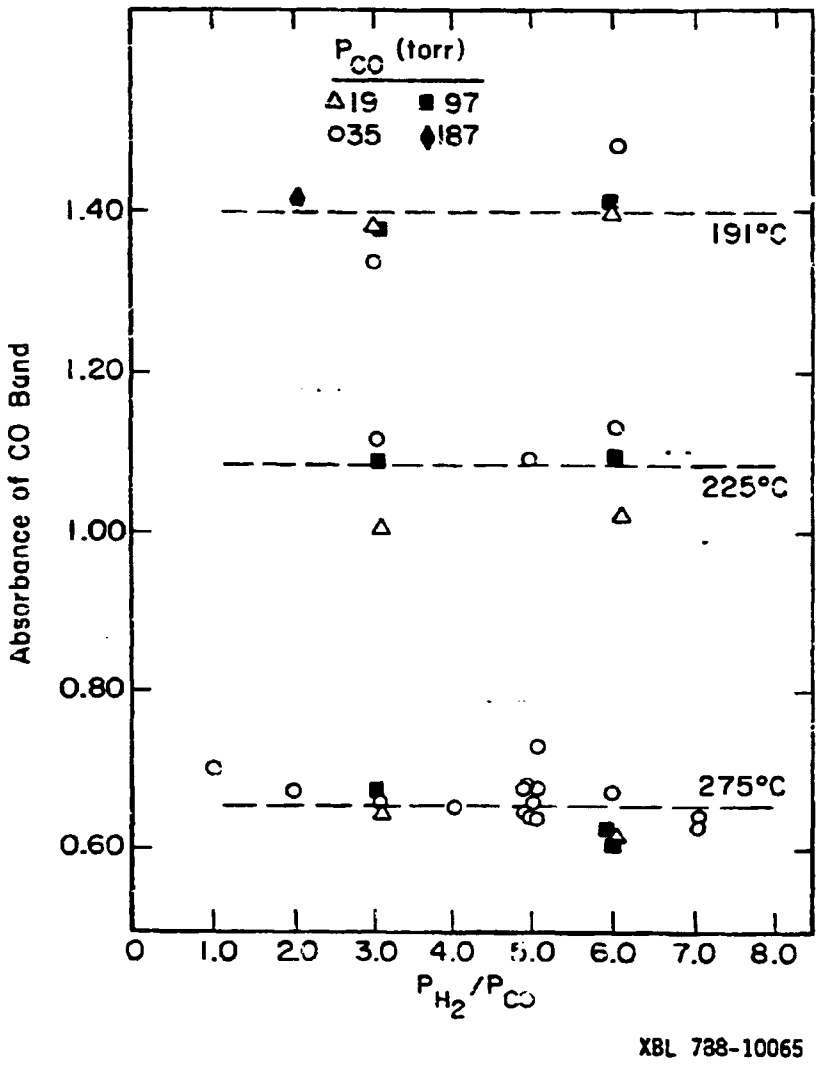

Figure 13. CO band absorbance as a function of CO partial pressure. H_2/CO ratio, and temperature

assigned to C-H stretching vibrations in methyl groups while the two more intense peaks at 2910 and 2845 cm^{-1} can be assigned to symmetric and asymmetric C-H vibrations in methylene groups (48).

To determine whether the observed C-H stretching frequencies might be due to the adsorption of hydrocarbon products on either the Ru or the support a gas mixture containing CO, CH_4, C_2H_4, C_2H_6, C_3H_6, C_3H_8, and CO_2 was passed over the catalyst at 191°C. No absorbtion bands were observed. This indicates that the hydrocarbon adspecies giving rise to the bands in the vicinity of 2900 cm^{-1} are not reaction products adsorbed from the gas phase, but rather adspecies formed during the course of the reaction.

A number of experiments were performed to determine the stability and reactivity of the adsorbed hydrocarbon species and their possible role in the formation of reaction products. In the first experiment a mixture of CO and H_2 was fed to the reactor, maintained at 191°C for 1 hr. The feed was then switched to a CO and D_2 mixture for 1 hr and then finally back to the original feed. It was observed that the bands at 2950, 2910, and 2845 cm^{-1} remained unchanged upon substitution of D_2 for H_2 but that a new set of bands were formed at 2210, 2180 and 2090 cm^{-1}, corresponding to the fully deuterated forms of the hydrocarbon adspecies. Upon return to the feed containing H_2, the bands associated with the deuterated structures stopped growing and the bands corresponding to the hydrogen containing structures resumed their growth.

In the second experiment, a run was first carried out at 191°C. At the end of the run, the flow of H_2 was stopped and the flow of CO and He continued until H_2 had been eluted from the reactor. The CO flow was then terminated and CO was eluted from the reactor by a flow of He. Spectra of the surface taken after the elution of H_2 and CO are shown in Fig. 14. Spectrum b is identical to that recorded under reaction conditions. No change in the spectrum is observed following the elution of H_2 (spectrum c). Spectrum d taken after the elution of CO shows that the CO band has shifted to 1940 cm^{-1} and diminished somewhat in intensity. The shift in the CO band frequency from 2030 cm^{-1} to 1940 cm^{-1} suggests that a fraction of the CO monolayer has desorbed and that the remaining adsorbed CO is strongly bonded, possibly in a bridged fashion (49). It is important to note, however, that the adspecies responsible for the hydrocarbon bands are stable even in the absence of gas phase H_2 and CO.

Following the elution of CO in the experiment just described, a flow of H_2 in He was introduced into the reactor. Spectra taken subsequently show that the bands associated with the hydrocarbon species and the CO band are rapidly hydrogenated once CO is removed from the catalyst surface.

3. Reduction of Carbonaceous Residues

Following each steady-state experiment the flow of CO to the reactor was stopped but the flow of H_2 and He was continued. The purpose of this procedure was to flush the

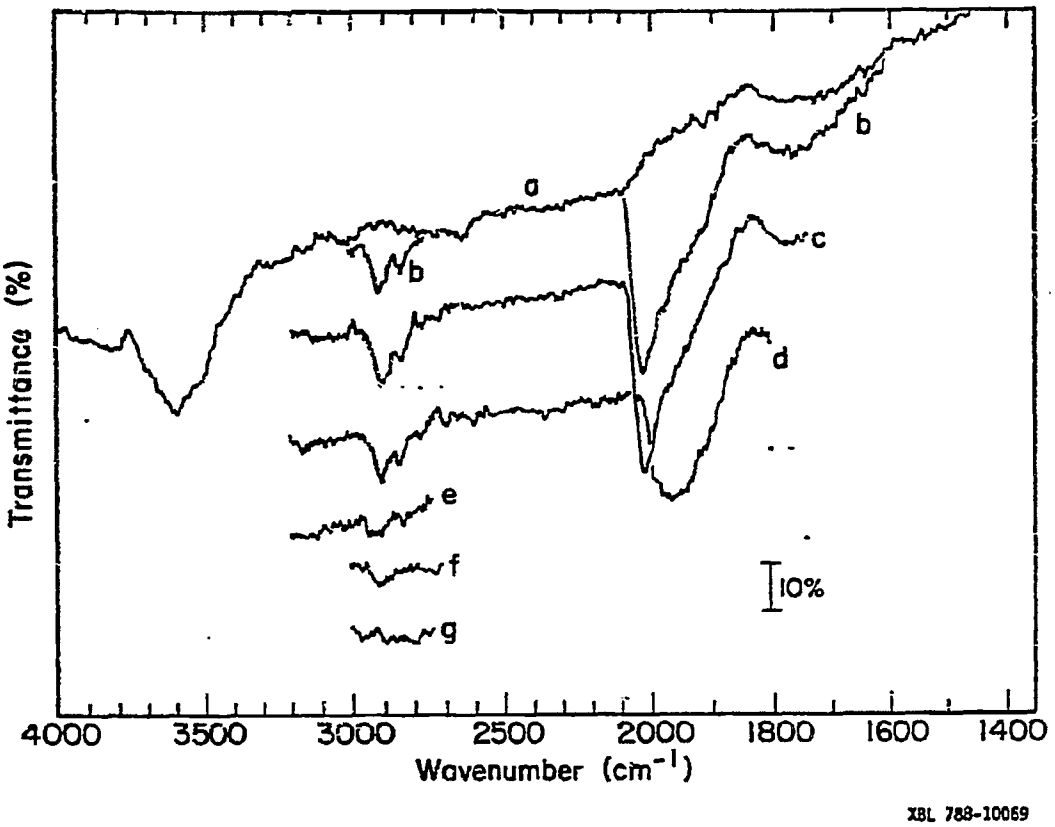

Figure 14. Infrared spectra showing reactivity of hydrocarbon adspecies: a) background; b) during reaction at T = 191°C, P_{CO} = 195 torr, and P_{H_2}/P_{CO} = 2; c) following elution of H_2; d) following elution of H_2 and CO; e) 2.5-min following admission of H_2/He mixture; f) 4.5 min following admission of H_2/He mixture; g) 7.5 min following admission of H_2/He mixture.

reactor of CO and to remove any carbonaceous residues from the catalyst by reaction with H_2. Reactor effluent compositions and infrared spectra taken during this period provided important information with regard to the identity and reactivity of the species present on the catalyst surface at the end of a run.

Figures 15 and 17 show the relative absorbance of the CO band, appearing at 2030 cm^{-1}, as a function of the time since termination of the CO flow. The curves for all four runs are qualitatively similar. Initially the relative absorbance remains constant at unity and then at a well defined moment falls rapidly to zero. Similar patterns were also observed at 225 and 275°C. As the temperature is increased the time at which the CO band disappears becomes shorter.

To interpret the curves of CO absorbance versus time, it is necessary to know the time dependence of the CO partial pressure in the gas phase. Unfortunately, over the time span shown in Figs. 15 and 17 only one gas sample could be analyzed. The CO partial pressures determined from these analyses divided by the steady-state CO partial pressures are indicated by the isolated data points. Since there is so little composition data, an upper bound on the CO partial pressure is shown as well. The straight lines appearing in Figs. 15 and 17 are given by

$$P_{CO}(t)/P_{CO}(0) = e^{-t/\tau} \qquad (5)$$

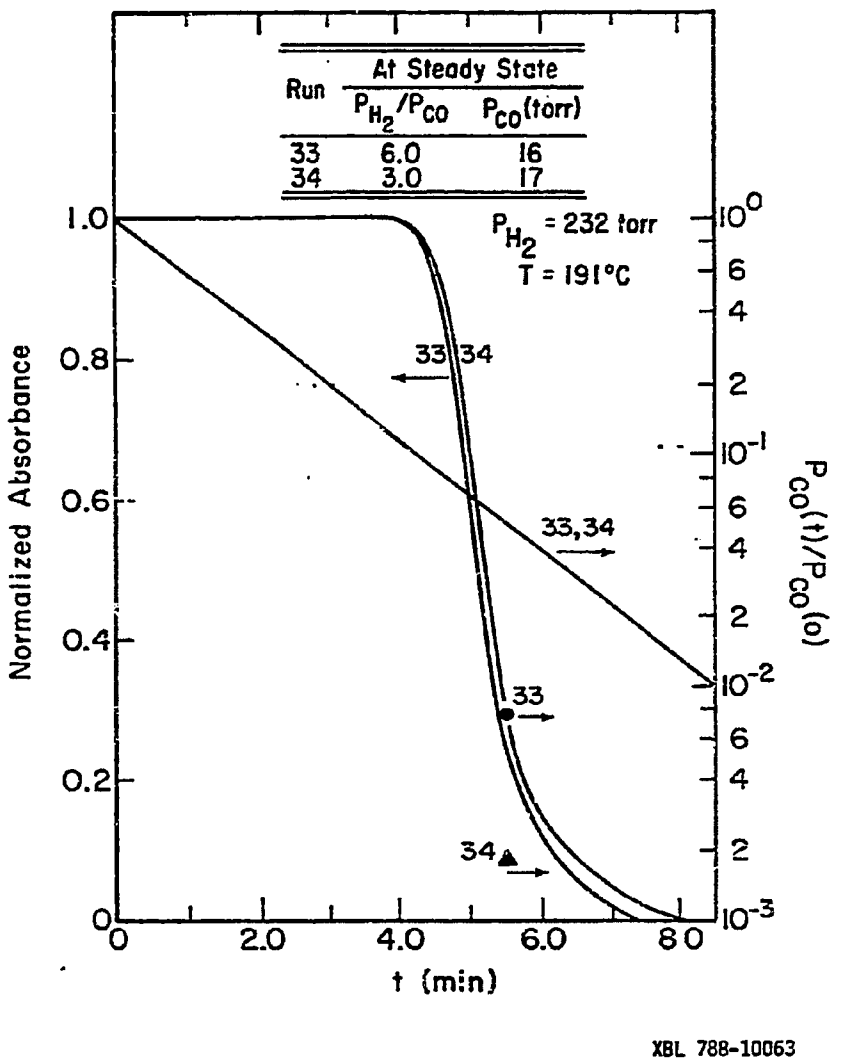

Figure 15. Response of CO band absorbance and CO partial pressure during catalyst reduction following steady state reaction: P_{CO} = 16 torr

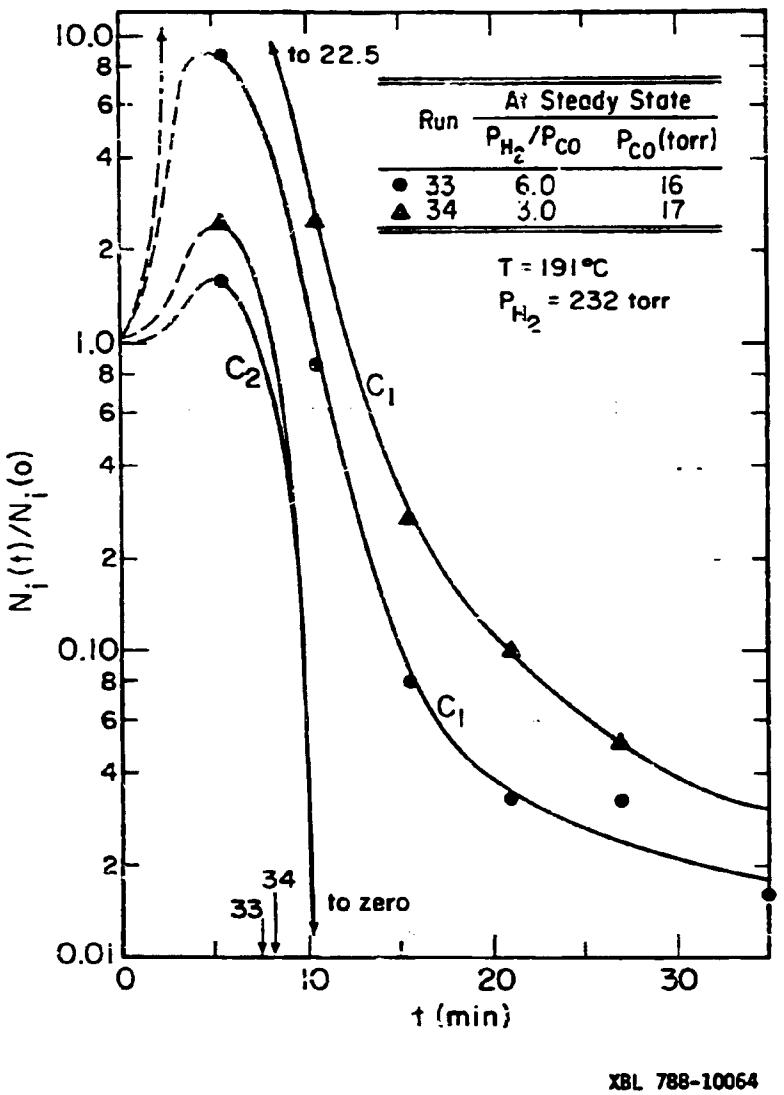

Figure 16. Relative rates of methane and ethane production during catalyst reduction following steady state reaction: P_{CO} = 16 torr (Arrows indicate the time at which the CO band absorbance goes to zero.)

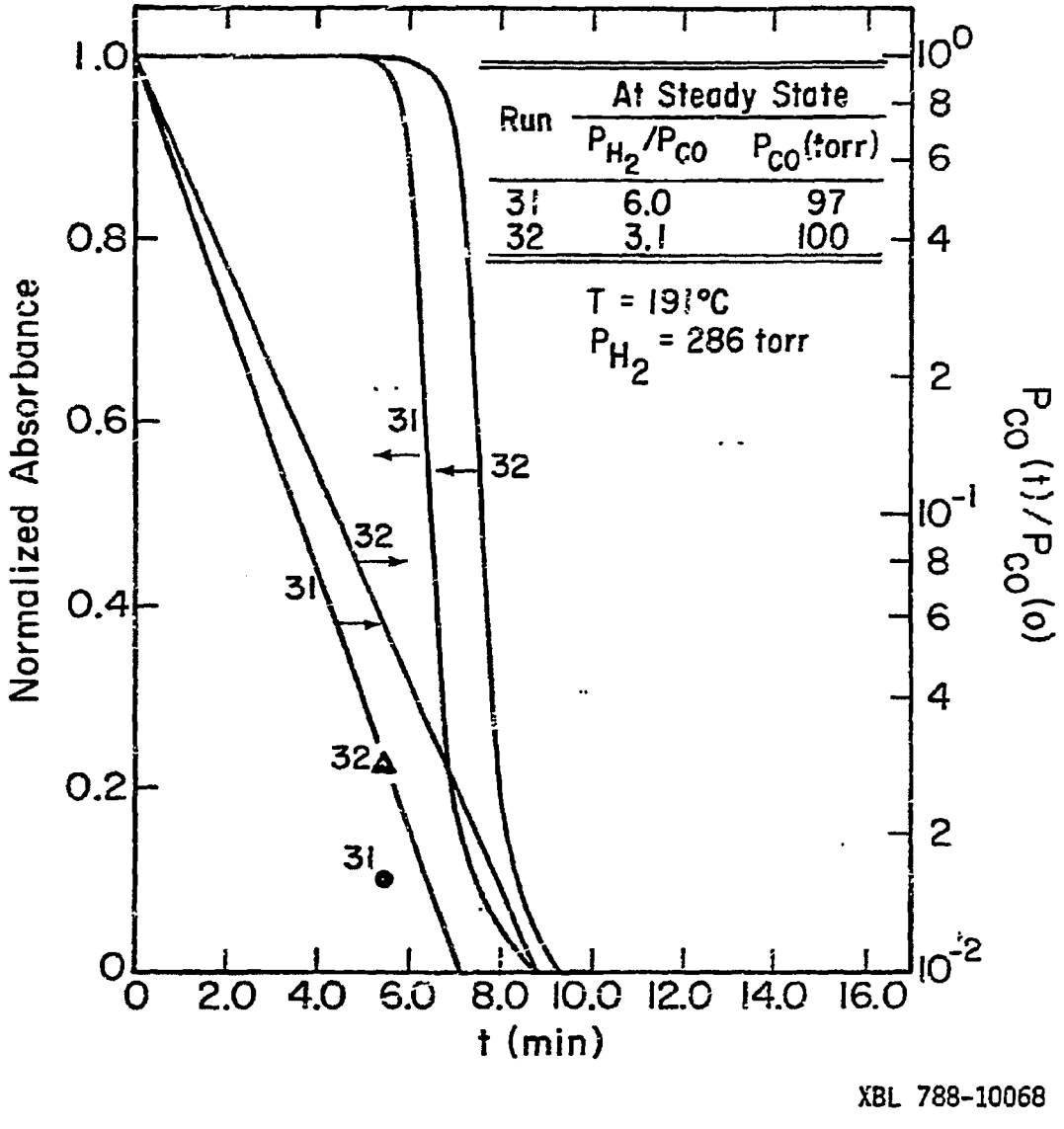

Figure 17. Response of CO band absorbance and CO partial pressure during catalyst reduction following steady state reaction: P_{CO} = 100 torr

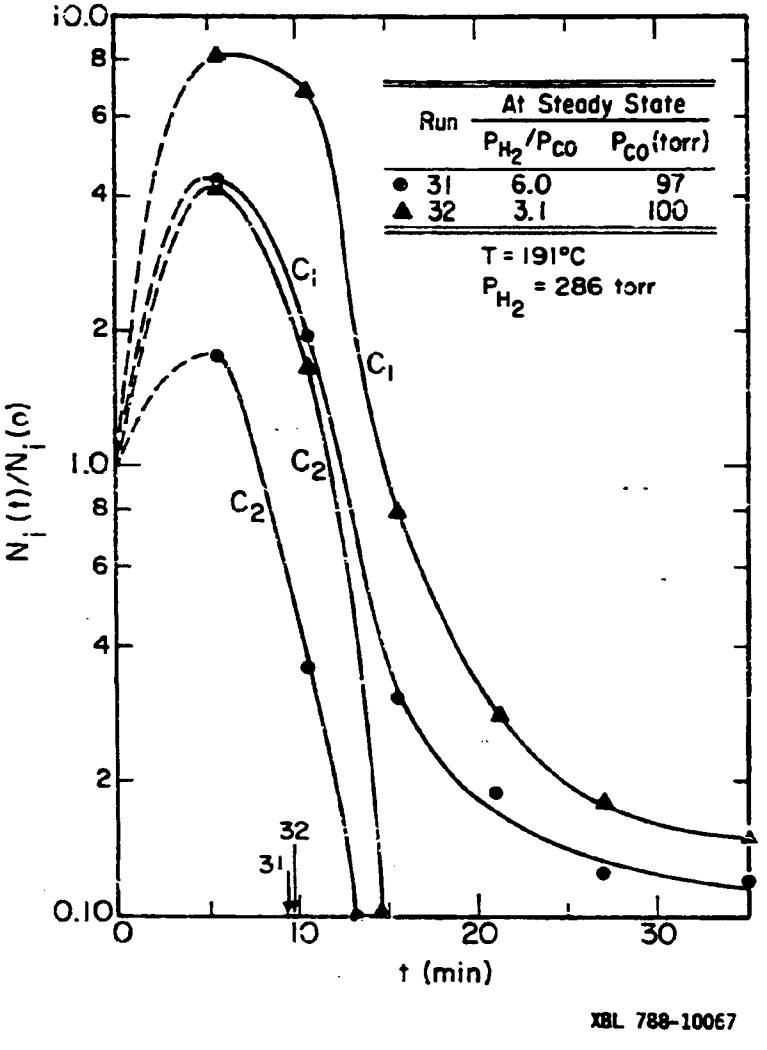

Figure 18. Relative rates of methane and ethane production during catalyst reduction following steady state reaction: P_{CO} = 100 torr. (Arrows indicate the time at which the CO band absorbance goes to zero.)

which represents the time dependence of a nonreacting component eluted from a well-stirred vessel (37). The parameter τ in eqn. 5 represents the reactor space time (typically 1.6 min). The location of the measured values of $P_{CO}(t)/P_{CO}(0)$ show that the CO partial pressure falls off more rapidly than predicted by eqn. 5, thereby indicating that a fraction of the CO reacts as it is eluted.

The curves of relative CO absorbance can now be understood by recognizing that as long as the CO partial pressure is sufficiently high, the Ru surface remains essentially saturated with CO and the relative absorbance is unity. Once the CO partial pressure becomes significantly less than a torr the readsorption rate can no longer keep up with the rate of CO removal from the surface and the relative absorbance falls. Consistent with this picture we observe that the time at which the decay in absorbance begins depends upon the CO partial pressure used at steady state but is independent of the steady-state H_2/CO ratio. The slight displacement in curves for the two runs shown in Fig. 17 is totally due to the difference in the flow rates of the H_2/He streams used in these runs.

The decay in CO absorbance which occurs at low CO pressures could either be due to desorption or reaction with H_2. The first of these possibilities can be excluded based upon experiments in which He alone was used to elute the CO. During these experiments the CO absorbance remained at near saturation levels even though the CO partial pressure was

reduced to the order of 10^{-3} torr. On the other hand, when H_2 was present in the eluting gas, the chemisorbed CO could be removed from the surface at CO partial pressures of the order of one torr.

Figures 16 and 18 show the relative rates of methane and ethane production during reduction. For each run the curves for both components pass through a maximum at about the same time that the CO absorbance goes to zero (as indicated by the vertical arrows). Beyond the maximum, the relative rate of methane formation falls off gradually but the relative rate of ethane formation declines rapidly to zero. While the curves for methane shown in Figs. 16 and 18 terminate at 35 min., data were usually collected for 125 min. The magnitude of the maxima in the methane and ethane curves and the level of the slowly decaying portion of the methane curve increase as either the steady-state partial pressure of CO or the H_2/CO ratio is decreased. It should be noted, however, that the absolute rate of methane production measured at 35 min increases with both CO partial pressure and H_2/CO ratio.

The observation of hydrocarbon formation long after CO has been eluted from the gas phase and removed from the catalyst surface is enhanced by increasing the steady-state partial pressure of CO and decreasing the ratio of H_2/CO. Figure 19 illustrates the rates at which methane and ethane are formed during reduction following a run at 191°C in which the feed partial pressure of CO was 195 torr and the

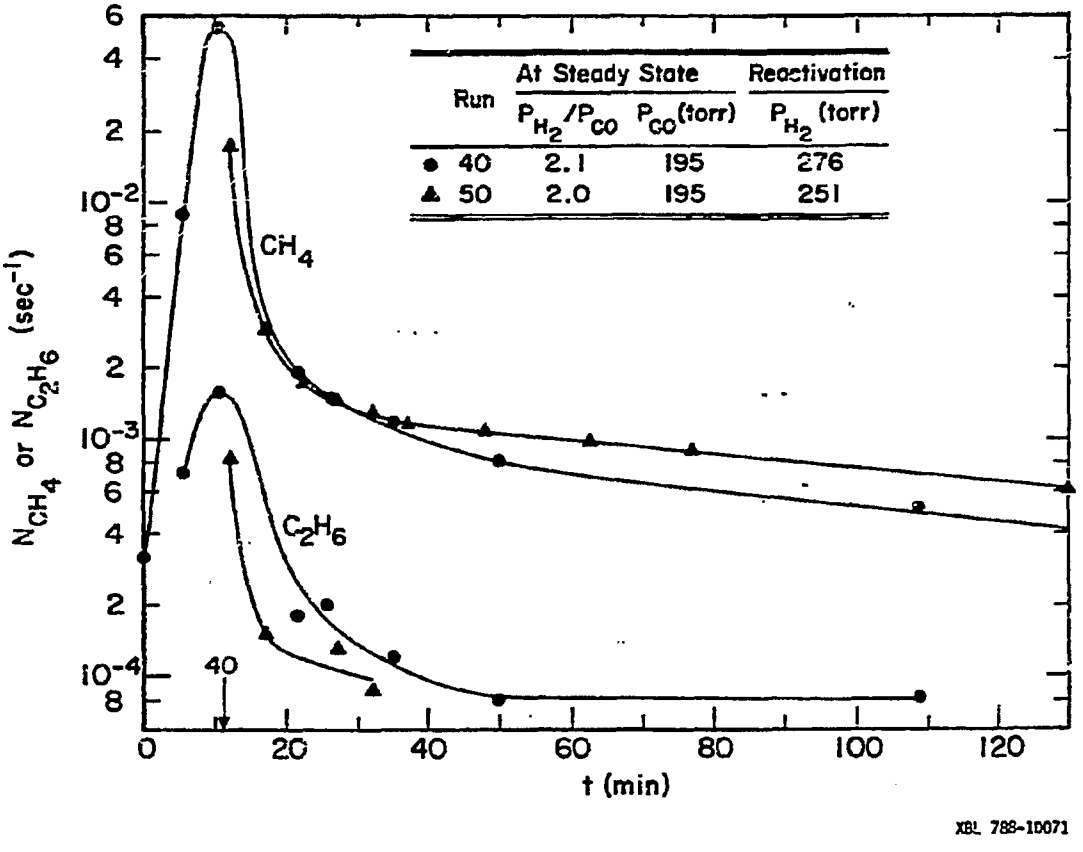

Figure 19. Absolute rate of methane and ethane production during catalyst reduction following steady state reaction: P_{CO} = 195 torr. (-●- CO eluted by H_2/He stream; -▲- CO eluted by He prior to introduction of H_2/He stream)

H_2/CO ratio was 2.0. In contrast to the results shown in Figs. 16 and 18, ethane formation continues for a long time beyond the point at which CO is present either in the gas phase or on the surface of the catalyst. While not shown in Fig. 19, a small amount of propane was also observed during the reduction period. It is interesting to note that when the catalyst was operated at steady state neither ethane nor propane was observed, and only methane and propylene were detected.

The shape of the curves appearing in Figs. 16, 18, and 19 can be interpreted in the following fashion. Upon cessation of the CO flow, the H_2 partial pressure in the H_2/He feed stream is set to about 290 torr. This causes the CO partial pressure to steadily decline while the H_2 partial pressure changes from the value held during steady state to that in the H_2/He stream. The net result is a very rapid increase in the H_2/CO ratio of the gas within the reactor. In response to this change, the rate of hydrocarbon production increases. For the case of methane the response to the decrease in CO partial pressure is predicted by eqn. 4. Consistent with the proposed interpretation, we observe that the extent to which the steady-state rate of hydrocarbon formation is surpassed depends upon the CO partial pressure and the H_2/CO ratio maintained during the steady-state period. The lower the CO partial pressure or the H_2/CO ratio, the greater is the net rise of the steady-state reaction rate.

The appearance of a maxima in the curves of relative rate of hydrocarbon formation closely coincides with the complete elution of CO from the reactor gas space and the elimination of CO from the catalyst surface. This feature suggests that at very low CO partial pressures the rate of hydrocarbon formation becomes positive order in CO, in response to CO adsorption becoming a rate limiting step.

The continued formation of hydrocarbon products, long after CO has been excluded from the reactor and the catalyst surface, is the most interesting characteristic of the data shown in Figs. 16, 18, and 19. In addition, it is seen that the rate of methane formation is comparable to the steady-state rates for extended periods of time. These observations suggest that the hydrocarbon products observed are formed by hydrogenation of a carbonaceous species on the catalyst surface, and that these same species may be responsible for product formation under steady-state reaction conditions.

To further confirm the idea that hydrogenation of carbonaceous residues present on the catalyst surface could produce methane and ethane, the following experiment was carried out. Upon completion of a steady-state run at 191°C, first H_2 and then CO was eluted from the reactor. A flow of H_2 in He was then introduced. Infrared spectra taken after the addition of H_2 showed that within 4 min. all of the adsorbed CO had been removed from the surface. The subse-

quent rates of methane and ethane formation were observed as functions of time and are shown by the triangular data points in Fig. 19. The curve is shifted by 7 min. to coincide with disappearance of adsorbed CO for both experiments. It is apparent that the initial rate of methane production is nearly a hundred-fold higher than that observed at steady state and that even after 125 min of reaction the rate is a factor of two greater than the steady-state rate. While no ethane was produced during the steady-state period, it is seen that a significant amount of ethane appears during the hydrogenation of the carbonaceous residue. Adsorption of the product gases, formed during the first 5 min of reduction, on activated carbon and subsequent mass spectrometric analysis of the desorbed gases revealed that small amounts of propane were also produced during the early stages of reduction.

In an attempt to obtain measurable quantities of propane in the absence of CO an experiment similar to that just discussed was performed. In the new case the total reduction flow rate was reduced, while maintaining all other variables constant. If the rates of reduction are the same, the molar concentration of products will increase as the flow rate decreases. The data is presented in Fig. 20. The curves for both experiments are in very good agreement. (In Fig. 20 the curves are plotted against the experimental time.) When the volumetric flow rate is decreased detectable quantities of propane are present. The sample taken at 16 min. contain propane at the lower limit of detection,

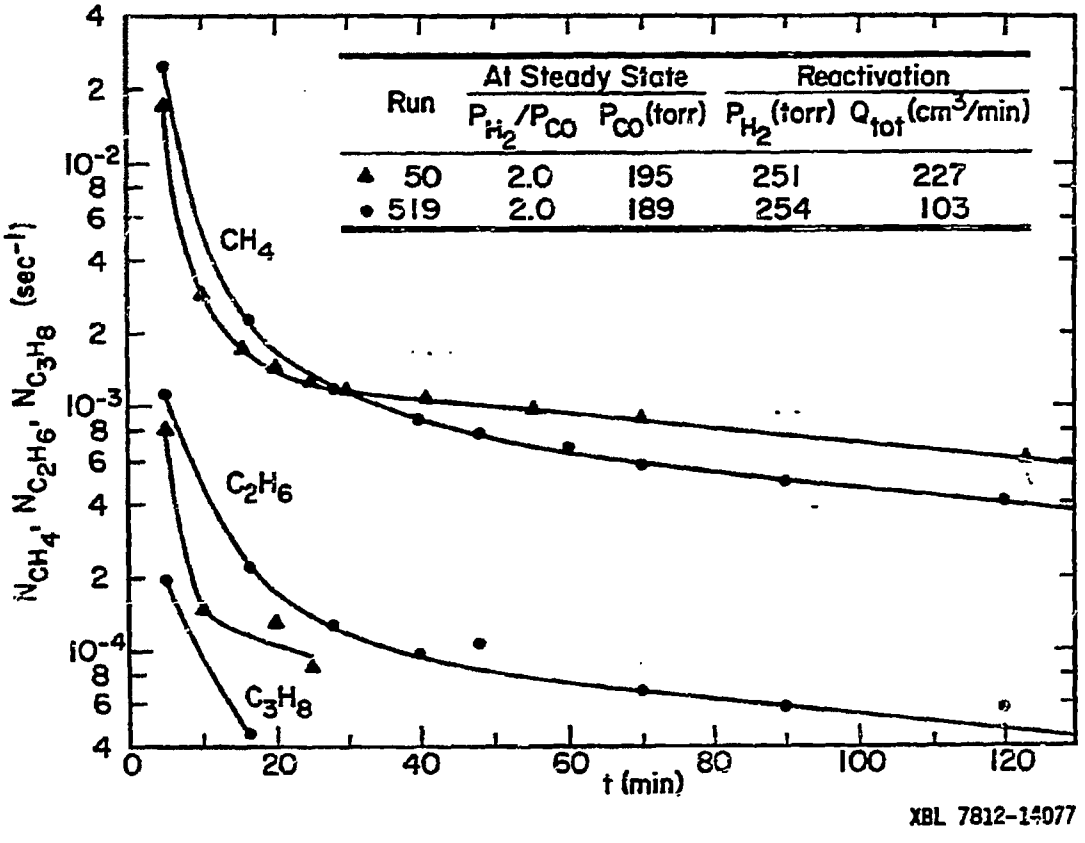

Figure 20. Absolute rate of methane, ethane and propane production during catalyst reduction following steady-state reaction: P_{CO} = 195 torr. CO eluted by He prior to introduction of H_2/He stream. (-▲- total H_2/He flow rate of 227 cm^3/min; -●- total H_2/He flow rate of 103 cm^3/min)

therefore it is not possible to tell how long it continues to be produced. This data confirms that both ethane and propane are produced in significant quantities in the absence of chemisorbed CO.

The total amounts of carbon removed from the catalyst as methane are shown in Table 5. These figures were obtained by integrating the production of each component. Integration was started at a point 2.3 space times (approximately 4 min) beyond the time at which the CO band disappeared from the spectrum and was terminated at the time when the rate of product formation became negligibly small. The total number of moles of carbon removed from the catalyst is in most instances greater than the number of Ru surface sites (7.9×10^{-6} moles) and is clearly dependent upon the reaction conditions under which the carbon is deposited. The table shows that for a constant inlet partial pressure of CO and H_2/CO ratio, the amount of carbon deposited increases with the reaction temperature. In addition, at a constant temperature, the carbon deposited increases with both the inlet partial pressure of CO and the H_2/CO ratio. It is also evident that the amount of carbon deposited is independent of the duration of a steady-state run carried out at 191°C.

To determine whether the amount of carbon deposited under reaction conditions was different from that deposited upon exposure of the catalyst to CO alone, a run was carried out in which the catalyst was maintained at 191°C in a CO/He

Table 5

Integrated Product Yields Obtained

During Reduction of Carbonaceous Residues

Run	Steady-State Conditions				Reduction Conditions	Integrated Product Yield	
	T(°C)	P_{CO}(torr)	P_{H_2}/P_{CO}	t(min)	P_{H_2}(torr)	CH_4 (μmoles)	C_2H_6 (μmoles)
46	275	100	3	70	301	34.7	-
45	225	101	3	70	299	16.0	-
32	191	100	3	70	281	16.2	-
31	191	97	6	70	292	33.3	-
33	191	16	6	70	244	2.6	-
34	191	17	3	70	220	1.4	-
35	191	186	2	70	304	48.6	5.4
40	191	195	2	120	276	49.2	4.4
519	191	189	2	120	254	49.5	5.3
50	191	195	2	90	251	43.9	-
41	191	201	1	90	232	15.7	-
-	191	223	0	70	222	2.5	-

flow for 70 min. Following this exposure, the flow of CO was discontinued and a stream containing H_2 in He was introduced into the reactor. Table 5 shows that the amount of carbon removed as methane is considerably smaller than that observed after a reaction run.

B. Discussion

The kinetics of methane formation reported here are correlated by eqn. 4, using the values of X,Y,A and E given in Table 6. Similar rate expressions have been reported by Dalla Betta et al. (8) and Vannice (11,12) and the rate parameters found in those studies are also shown in Table 6. There is general agreement among all three investigations concerning the order with respect to H_2 partial pressure, but the order with respect to CO shows a wider spread. The results of this investigation and that of Vannice indicate a nearly inverse half order dependence while that of Dalla Betta et al. favors a roughly inverse first order CO dependence. The agreement with regard to the apparent activation energy is very good, all three groups reporting a value of about 24 Kcal/mole. There is greater disagreement, however, concerning the magnitude of the pre-exponential, A. Differences in this parameter are very hard to reconcile since the specific activity of Ru catalysts can depend upon the dispersion (7) and the accuracy with which the Ru surface area was measured (17).

Table 6

Rate Parameters Appearing in Eqn. 4

	This Study	Vannice (5,12)	Dalla Betta et al. (8)
Catalyst	5% Ru/SiO_2	5% Ru/Al_2O_3	1.5% Ru/Al_2O_3
A(sec^{-1} $torr^{y-x}$)	5.6×10^6	7.4×10^5	3.1×10^5
E(Kcal/mole)	24.1	24.2 $\pm$ 1.2	24
X	1.5	1.6 $\pm$ 0.1	1.8
Y	-0.6	-0.6 $\pm$ 0.1	-1.1

The infrared spectra taken under reaction conditions show that at a fixed temperature neither the CO partial pressure nor the H_2/CO ratio affects the frequency or intensity of the CO band appearing at 2030 cm^{-1}. In addition the band position and intensity are identical to those observed when CO is adsorbed in the absence of H_2. These observations differ from those of Dalla Betta and Shelf (18). In their investigation with an alumina-supported Ru catalyst it was found that the CO band which appeared at 2043 cm^{-1} in the absence of H_2 shifted to 1996 cm^{-1} when H_2 was present in 3 to 1 ratio with CO. The occurence of a frequency shift was used to argue that adsorbed H_2 contributed to a weakening of the C-O bond. The absence of a shift in the CO band position when CO and H_2 are coadsorbed on a silica-supported Ru catalyst might be regarded as an indication of the differences between alumina and silica-supported Ru. However, the nature of these differences cannot be explained at this time.

The results presented in Fig. 13 show that the intensity of the CO band decreases as the temperature increases but that the band intensity is essentially independent of CO partial pressure and H_2/CO ratio at each temperature. These observations can be interpreted by comparison of the data in Fig. 13 with CO adsorption isotherms. Figure 21 illustrates a series of isotherms measured gravimetrically

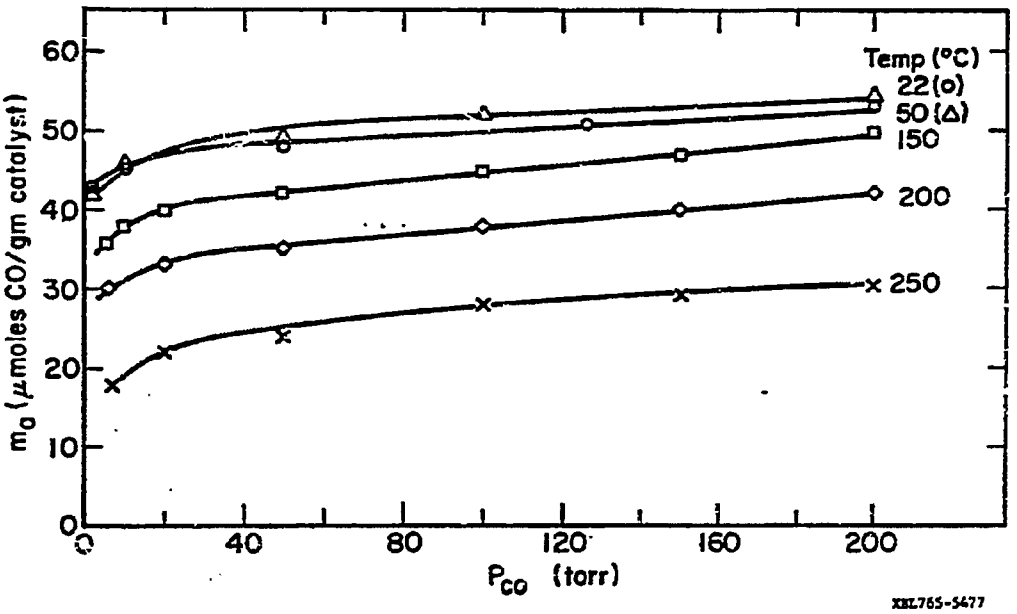

Figure 21. CO adsorption isotherms (50)

on a silica-supported Ru catalyst very similar to that used in the present studies (50). For a fixed CO pressure the coverage by adsorbed CO is seen to be a strong function of temperature. By contrast, CO coverage changes more slowly as the CO pressure is increased at a fixed temperature. The decrease in CO absorbance with increasing temperature, seen in Fig. 13, can, thus, be ascribed to a decrease in the coverage by adsorbed CO. The absence of a dependence on CO band intensity on H_2/CO for a fixed CO partial pressure suggests that H_2 adsorption does not interfere with CO adsorption and that the reaction of chemisorbed CO is slow by comparison with desorption. As a result, the presence of H_2 does not influence the chemisorption equilibrium for CO. The failure to observe an increase in CO band intensity with CO partial pressure is surprising in view of the adsorption data shown in Fig. 21. A possible explanation may lie in the decision to use maximum absorbance as a measure of CO coverage rather than integrated band absorbance.

The hydrocarbon bands in the vicinity of 2900 cm^{-1} which have been observed in this work are very similar to those seen by King (19) on silica-supported Ru and by Dalla Betta and Shelef (18) and King (19) on alumina-supported Ru. In view of the stability and reactivity patterns exhibited by the species responsible for the observed bands it seems reasonable to conclude that these species are present on the Ru rather than on the support. While it is not possible

to establish the structure of the hydrocarbon species, it is of interest to note that Eady et al. (17) have recently reported the formation of various Ru clusters containing carbene, ethylidene, ethylidyne, and ethylenic structures. These products were formed by reaction of $Ru_3(CO)_{12}$ with $Na[BH_4]$. It is conceivable that the species formed in the present work are similar to those observed by Eady et al. The occurrence of hydrocarbon species surrounded by adsorbed CO might explain the stability of these species to hydrogenation under reaction conditions and the ease which they can be hydrogenated once the adsorbed CO is removed from the Ru surface.

The results presented in Table 5 show that under reaction conditions the catalyst maintains a carbon reservoir in excess of a monolayer. Furthermore, as seen in Figs. 16, 18, 19 and 20 this carbon is very reactive and in the absence of CO on the surface can be hydrogenated to produce methane, ethane and propane. The rate of methane production is equivalent to or greatly in excess of that measured under steady-state conditions. These observations lead to the consideration of carbon as an important intermediate not only for methane formation but also for the synthesis of higher molecular weight products. In this context it is important to discuss the origin of the carbon deposit, the influence of reaction conditions on the magnitude of the deposit, and the mechanisms by which carbon is converted to methane and other hydrocarbon products.

Rabo et al. (27), McCarty et al. (22), and Low and Bell (25) have observed that carbon deposition can occur on the surface of Ru during CO adsorption at temperatures above about 150°C (25). This process is accompanied by the formation of CO_2 and is believed to occur by the following steps (27):

1. $CO + S \rightleftharpoons CO_s$
2. $CO_s + S \rightleftharpoons C_s + O_s$
3. $O_s + CO \rightarrow CO_2$

McCarty et al. (22) have estimated that the equilibrium constant for reaction 2 is unfavorable due to the high endothermicity of the reaction (21 Kcal/mole) and that, as a result, reaction 3 plays an important role in shifting the equilibrium towards the formation of carbon. When H_2 is present in addition to CO, the removal of surface oxygen is further enhance by reaction 4

4. $O_s + H_2 \rightarrow H_2O$

Both reactions 3 and 4 have been observed experimentally to proceed preferentially via Rideal-Eley type processes over Pt when CO or H_2 is present at moderate partial pressures [e.g. (51-57)] . While similar observations have not been made for Ru, it has been assumed that oxygen removal occurs by a Rideal-Eley process for this catalyst as well. BEBO estimates of the activation energies for reactions 3

and 4 occurring over Ru give 17 and 0 Kcal/mole respectively (58,59). As a result, it is anticipated that for identical fluxes of reducing agent reaction 4 will be much more rapid than reaction 3 in effecting the removal of adsorbed oxygen atoms. Supporting this expectation is the observation that H_2O rather than CO_2 is observed as the major oxygen containing product under all synthesis conditions studied in this work. It is also seen in Table 5 that the amount of carbon deposited on the catalyst is significantly greater when CO and H_2 are present together than when CO is present alone.

The observation of greater than monolayer accummulations of carbon taken together with the observation that the surface coverage by chemisorbed CO is unaffected by the accummulation of carbon suggest that only a small fraction of the total carbon is present on the Ru surface. Since Ru does not form bulk carbides (66) and has only small solubility for carbon (60) one can not rationalize the storage of large quantities of carbon within the Ru crystallites. This leaves the possibility that the carbon may be present on the silica support or in filaments extending from the Ru surface. Unfortunately, presently available information is insufficient to determine the exact nature of the carbon deposit.

A plausible mechanism for the hydrogenation of surface carbon to form methane is shown below. This reaction

5. $H_2 + 2S \rightleftharpoons 2H_s$

6. $C_s + H_s \rightleftharpoons CH_s + S$

7. $CH_s + H_s \rightleftharpoons CH_{2s} + S$

8. $CH_{2s} + H_s \rightleftharpoons CH_{3s} + S$

9. $CH_{3s} + H_s \rightarrow CH_4 + 2S$

sequence is nearly identical to that proposed by Wagner (61) to explain the formation of methane from carbon dissolved in γ-iron. If it is assumed that reaction 9 is rate limiting for the synthesis of methane; that reactions 1, 2 and 5 through 8 are at equilibrium; and that the catalyst surface is nearly saturated with chemisorbed CO, then the following expression is obtained for the rate of methane formation:

$$N_{CH_4} = k \frac{P_{H_2}^{1.5}}{P_{CO}} \qquad (6)$$

$$k = \frac{K_5}{K_1} (k_4 k_9 K_2 K_6 K_7 K_8)^{1/2} \qquad (7)$$

where k_i is the rate coefficient and K_i the equilibrium constant for the ith elementary reaction. Equation 6 has the same form as eqn. 4 and the exponent on the hydrogen

partial pressure is nearly identical to that found experimentally. The inverse first order dependence on CO partial pressure given by eqn. 6 is greater, however, than the nearly inverse square root dependence observed experimentally. Selection of other rate limiting steps within the proposed sequence not only fails to reduce the dependence on CO partial pressure but also causes the hydrogen partial pressure dependence to deviate from that observed experimentally.

A rate expression more representative of the experimental results can be obtained if it is postulated that the rate limiting step is reaction 8' shown below.

8'. $CH_{2s} + H_2 \rightarrow CH_4 + S$

Maintaining all of the previous assumptions, but substituting reaction 8' for reactions 8 and 9, the rate expression derived for methane formation becomes:

$$N_{CH_4} = k' \frac{P_{H_2}^{1.5}}{P_{CO}^{0.5}} \qquad (8)$$

$$k' = (k_8, k_4 K_5 K_6 K_7 / K_1)^{1/2} \qquad (9)$$

while eqn. 8 is in closer agreement with the observed rate expression than eqn. 6 there has been no experimental evidence to suggest that reaction 8' proceeds as written.

The processes by which two- and three-carbon hydrocarbons are formed are not revealed by these studies, but it has been established that these products can be formed in

absence of adsorbed CO. One possibility is that adsorbed carbene groups, formed via reaction 7, polymerize and react according to the following scheme:

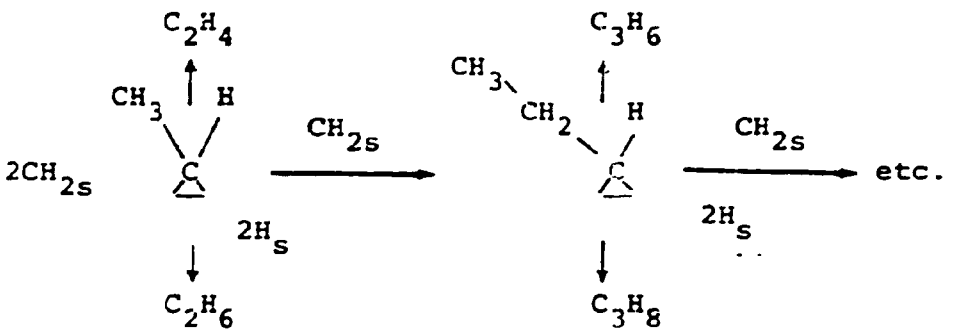

Carbenes have been observed as ligands in Os and Ru cluster complexes (17, 62) and in mononuclear Fe complex (63) and an ethyledene structure has recently been reported on the surface of Pt (64). Thus, it is not unreasonable to postulate these species as surface intermediates. Furthermore, given the known reactivity of gas phase carbenes and their metalorganic analogs it would appear likely that the chain propagation sequence proposed is possible.

The formation of olefins could occur by intramolecular hydrogen transfer within the appropriate carbene intermediate, followed by desorption. Some evidence supporting such a process can be derived from the reported chemistry of alkyl carbenes prepared from organometallic precursors (38). The observed preverential formation of propylene over ethylene could possibly result from the greater ease with which a hydrogen atom is transferred from the methylene group of propylidene compared to the transfer of hydrogen from the

methyl group of ethylidene. As an alternative one might propose that gas phase ethylene very rapidly reacts with surface carbene groups to form propylidene, in analogy to known gas phase chemistry. (65)

Finally, it is noted that the proposed propagation scheme can be used to predict a Schultz-Flory-type distribution of product molecular weights (34). To obtain such a distribution it is only necessary to postulate that steady-state concentrations exist for H_s and CH_{2s}, and that the rate coefficients associated with propagation, desorption to form olefins, and hydrogenation to form alkanes are independent of carbon number. Thus, for example, the experimental results on product distribution recently reported by Dautzenberg et al. (46) could be interpreted by the mechanism proposed here.

C. Conclusions

The results of the investigation have clearly shown that carbon produced by the dissociation of chemisorbed CO plays an essential role in Fischer-Tropsch synthesis over Ru. Under steady-state operation the catalyst maintains a carbon reservoir equilvalent to 1 to 6 Ru monolayers, the magnitude of which is dictated by temperature, CO partial pressure, and H_2/CO ratio. A major part of the carbon may be present on the support or attached to Ru crystallites in the form of filaments, since carbon accumulation does not influence CO chemisorption.

Hydrogenation of carbon accummulated on the catalyst readily produces methane, ethane, and propane. In the absence of chemisorbed CO, the rates at which these products are formed may greatly exceed the rates observed under steady-state synthesis conditions, leading to the conclusion that chemisorbed CO inhibits the adsorption of H_2. This conclusion is consistent with observation of an inverse order dependence of the steady-state methane formation rate on CO partial pressure as well as infrared observations, which indicate a near saturation coverage of the surface by chemisorbed CO. A mechanism for methane synthesis based on the hydrogenation of surface carbon provides a rate expression in good agreement with experimentally observed kinetics.

The presence of ethane and propane in the products formed by hydrogenation of the surface carbon in the absence of chemisorbed CO strongly suggests that this species does not participate directly in chain growth. Instead, it is proposed that propagation proceeds by polymerization of methylene groups to form alkylidenes which in turn undergo rearrangement to form olefins or hydrogenate to form alkanes. Efforts to observe synthesis intermediates by infrared spectroscopy have not been successful, indicating that the surface concentration of these species are below the detection limits of the technique.

IV. EVIDENCE FOR ALKYLIDENE INTERMEDIATES IN FISCHER-TROPSCH SYNTHESIS OVER Ru.

A. Introduction

Several recent studies dealing with Fischer-Tropsch synthesis over Ru (22, 25, 27) have shown that chemisorbed carbon, formed by the dissociation of adsorbed CO, will readily hydrogenate to form methane and higher molecular weight hydrocarbons. In the preceeding chapter it was further established that the synthesis of ethane and propane could be achieved in the absence of chemisorbed CO, suggesting that this species does not participate in chain propagation over Ru. As an alternative it was proposed that methylene groups, formed by the partial hydrogenation of chemisorbed carbon, polymerize to form alkylidenes, which, in turn, undergo rearrangement to form olefins or hydrogenation to form alkanes. Such a mechanism represents a modification of the carbide mechanism originally proposed by Fischer (4) and later elaborated by Craxford and Rideal (6).

While chain propagation via methylene polymerization has not been established, there is growing evidence for the bonding of alkylidenes with group VIII metals. For example, methylene and ethylidene have been reported as ligands in Ru (17) and Os (62,67) cluster complexes and in mononuclear Fe complexes (63,68). Ethylidene groups have also been observed on a Pt(111) surface (64).

This investigation was undertaken in an effort to find evidence for alkylidene species during Fischer-Tropsch synthesis over Ru. Since previous studies (18,19) had shown that reaction intermediates could not be observed by infrared spectroscopy, an effort was made to detect alkylidenes by their reaction with an olefin, added to the synthesis gas mixture. This approach was motivated by the known reactivity of gas phase alkylidenes towards olefins (65, 69) and recent reports (68, 70) that alkylidene ligands can be eliminated from metal complexes by reaction with olefins. The olefins used in this work were ethylene and cyclohexene.

B. Experimental Methods

The apparatus used for these studies has been described in Chapter II. For the experiments in which ethylene was added to the feed, the products were passed through a dry ice trap to remove water and then analyzed by a gas chromatograph containing a column packed with Porapak Q. When cyclohexene was added to the feed the products were frozen in a liquid nitrogen trap. Prior to analysis the frozen products were thawed and the hydrocarbons disengaged from water by extraction with diethyl ether. The ether solution was then analyzed in a Finnigan GC-MS, fitted with a glass capillary column (30 m long x .25 mm ID), coated with SP2100. The column was operated at 30°C for 2 min, followed by a temperature increase to 200°C at 3°C/min, and finally held at 200°C for 30 min.

Ethylene (99.5 %) and reagent grade cyclohexene were used without purification.

C. Results

1. Ethylene Addition

The addition of ethylene was carried out at 191°C using a CO partial pressure of 180 torr and a H_2/CO ratio equal to 2. After initiating the synthesis with H_2 and CO, 15 torr of ethylene was added to the feed. The flow of ethylene was terminated after 42 min and the synthesis was continued for an addition 40 min. Product compositions during the three phases of this experiment are given in Table 7.

Prior to the introduction of ethylene, the products are mainly methane and propylene. A smaller amount of ethane is evident and a trace of ethylene is observed. When ethylene is added to the feed the distribution of hydrocarbon products is altered. It should be noted that only 17% of the ethylene fed is converted. Upon elimination of ethylene from the feed gas, the product concentrations return approximately to their original levels. The decreases in product concentrations relative to those observed prior to the addition of ethylene can be ascribed to a slow deactivation of the catalyst.

The change in product composition upon introduction of ethylene must be examined carefully in view of the hydrocarbon impurities present in the ethylene. It is apparent from

Table 7

Change in Product Composition upon Addition of Ethylene to the Synthesis Feed Gas

Experimental Sequence	Component	Feed Composition (mole %)	Product Composition (mole %)
0-38 min Feed I (sample taken at 10 min)	CH_4	0	2.38×10^{-3}
	C_2H_4	0	$< 5 \times 10^{-4}$ (a)
	C_2H_6	0	9.49×10^{-4}
	C_3H_6	0	3.46×10^{-3}
	C_3H_8	0	0
38-80 min Feed II (sample taken at 50 min)	CH_4	2.14×10^{-2}	3.17×10^{-2}
	C_2H_4	1.78	1.47
	C_2H_6	5.52×10^{-2}	2.63×10^{-1}
	C_3H_6	7.11×10^{-3}	1.97×10^{-2}
	C_3H_8	0	1.01×10^{-3}
80-120 min Feed I (sample taken at 102 min)	CH_4	0	1.59×10^{-3}
	C_2H_4	0	$< 5 \times 10^{-4}$
	C_2H_6	0	$< 5 \times 10^{-4}$
	C_3H_6	0	2.85×10^{-3}
	C_3H_8	0	0

Feed I $H_2/CO/He$ @ mole% 46.2/23.2/balance

Feed II $H_2/CO/C_2H_4/He$ @ mole% 45.8/22.9/1.8/balance

(a) Lower detectable limit

Table 7 that about 12% of the ethylene is hydrogenated to ethane. The high activity of Ru for this reaction is substantiated by the results shown in Table 8, which indicate that in the absence of CO 97% of the ethylene is converted to ethane. The increase in methane concentration above the impurity level present in the ethylene can be ascribed to a partial hydrogenolysis of the ethane formed from ethylene. This interpretation is supported by the data in Table 8.

The concentration of propylene in the products during the addition of ethylene is significantly larger than that observed prior to ethylene addition or as an impurity in the ethylene itself. If it is assumed that most of the propylene which enters as impurity is unreacted, then the increase in propylene production due to the presence of ethylene is a factor of 3.6. The appearance of some propane during the period of enhanced propylene production is probably the result of a partial hydrogenation of the propylene. Notice that in the absence of CO in the feed (Table 8) about 44% of the impurity propylene is converted to propane, the balance presumably undergoing hydrogenolysis to form methane and ethane.

2. Cyclohexene Addition

The synthesis conditions used for the experiments in which cyclohexene was added were chosen to maximize the rates of formation of C_2 and C_3 hydrocarbons. Based upon previous studies , a temperature of 225°C, a CO partial

Table 8

Product Composition Resulting from the Hydrogenation and Hydrogenolysis of Ethylene.

Component	Feed Composition (mole %)	Product Composition (mole %)
CH_4	3.47×10^{-2}	4.03×10^{-1}
C_2H_4	1.61	1.56×10^{-1}
C_2H_6	5.15×10^{-2}	1.56
C_3H_6	6.44×10^{-3}	0
C_3H_8	0	2.82×10^{-3}

Feed $H_2/C_2H_4/He$ @ mole % 57.6/1.6/balance

pressure of 177 torr, and a H_2/CO ratio of 3 were selected. After initiating the synthesis reaction, pulses of He saturated with cyclohexene at 25°C were injected into the feed stream to the reactor. Five pulses, each containing 0.5 mmoles of cyclohexene, were introduced at 30 min intervals. Following each injection, the reaction products were collected in a liquid nitrogen trap for a period of 10 min. During the remaining 20 min between injections the trap was bypassed. Use of this procedure maximized the concentration of products formed by reaction with cyclohexene in the trapped material.

A chromatogram of the synthesis products obtained prior to the injection of cyclohexene is shown in Fig. 22. The reconstructed ion count (RIC), displayed on the ordinate, represents the sum of all ion counts between 35 to 350 AMU for each scan, one scan being taken each second. Only that portion of the chromatogram appearing between scans 500 and 3200 is shown, to enhance the visibility of the smaller peaks. The regular sequence of large peaks appearing in Fig. 22 are identified, on the basis of mass fracturing patterns, as normal alkanes ranging from n-heptane at scan 417 to n-heptadecane at scan 3185. In the portion of the chromatogram below scan 500 peaks were observed for n-pentane and n-hexane. Cyclohexene and cyclohexane, when present, are also observed in this portion of the chromatogram, and it is estimated that about 13% of the injected cyclohexene

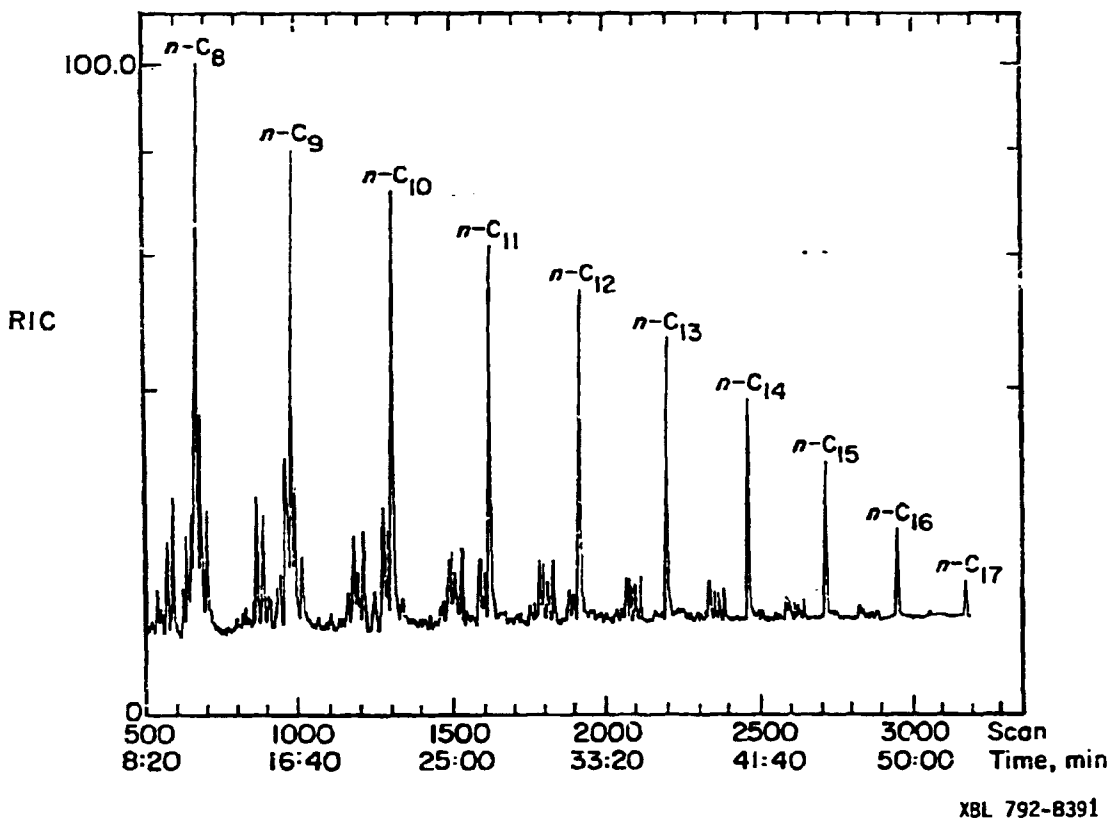

Figure 22. Chromatogram of the synthesis products

is converted to cyclohexane. The smaller peaks observed near each of the large peaks, seen in Fig. 22 are due to a variety of branched alkanes and both normal and branched alkenes. Figure 23 illustrates these peaks more clearly for the portion of the chromatogram between scans 400 and 1000. The identity of the peaks present in the region near n-octane are listed in Table 9.

The chromatogram of products obtained when cyclohexene is added to the feed stream is very similar to that obtained during synthesis in the absence of cyclohexene. The principal difference is that the intensities of the normal alkane peaks fall off more rapidly when cyclohexene is present. This point is brought out in Fig. 24 which shows a bar graph of peak intensities versus carbon number. Notice that with increasing carbon number the difference in peak intensities increases.

Figure 25 illustrates the portion of the chromatogram between scans 400 and 1000, for an experiment in which cyclohexene is present. Comparison of Figs. 23 and 25 clearly demonstrates that cyclohexene addition does not perturb significantly the nature or distribution of minor synthesis products.

Further examination of Fig. 25 reveals three peaks not present in Fig. 23. These features are located at scans 484, 560, and 746. A partially resolved peak is also seen at scan 852. An identification of these peaks was carried out by comparing the associated mass spectra with mass

BLANK PAGE

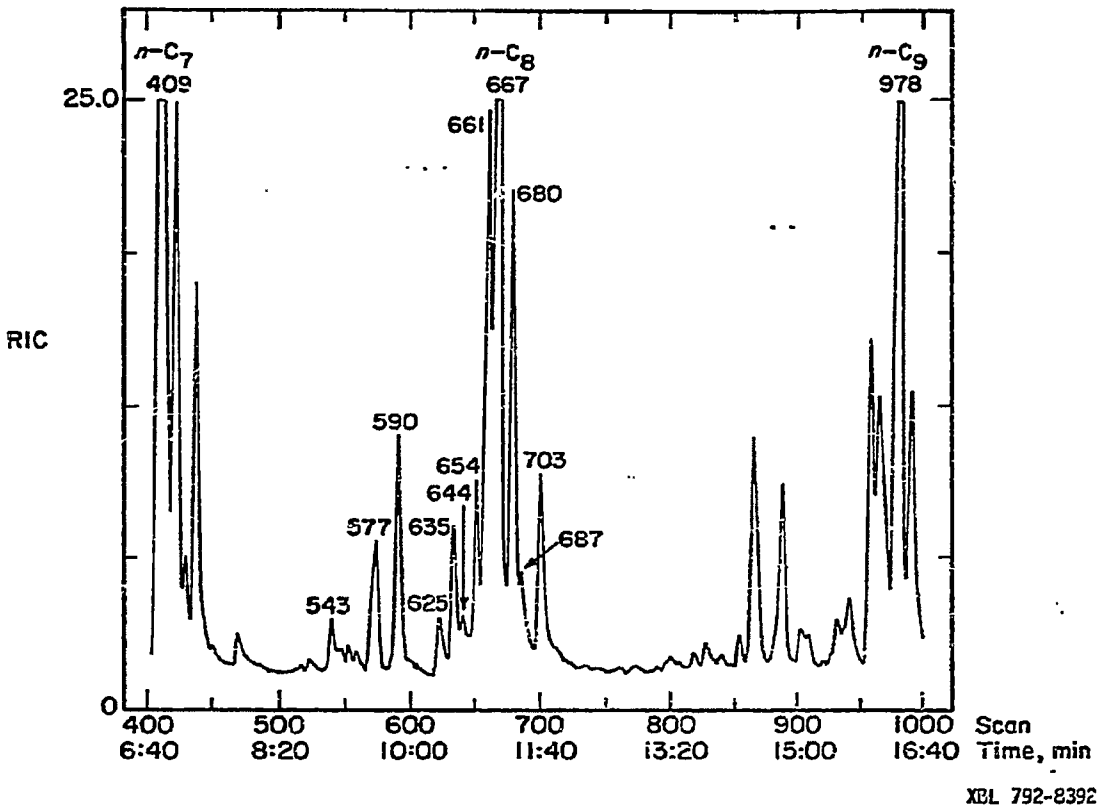

Figure 23. Chromatogram of the synthesis products

Table 9

Identification of Chromatographic Peaks

Compound	Location (scan no.) Fig. 23	Fig. 25
2,3-dimethyl-2-hexene	543	543
2-methyl heptane	577	582
3-methyl heptane	590	593
octene (4 or 2) [a]	625	627
1-octene	635	636
2-methyl-3-heptane	644	646
octene (4 or 2)	654	656
3-octene	661	663
octane	667	671
octene (2.4, or 1)	680	681
3-methylene heptane	689	692
octene (4 or 2)	703	703

(a) The Finnigan computer is unable to distinguish between the normal olefins shown.

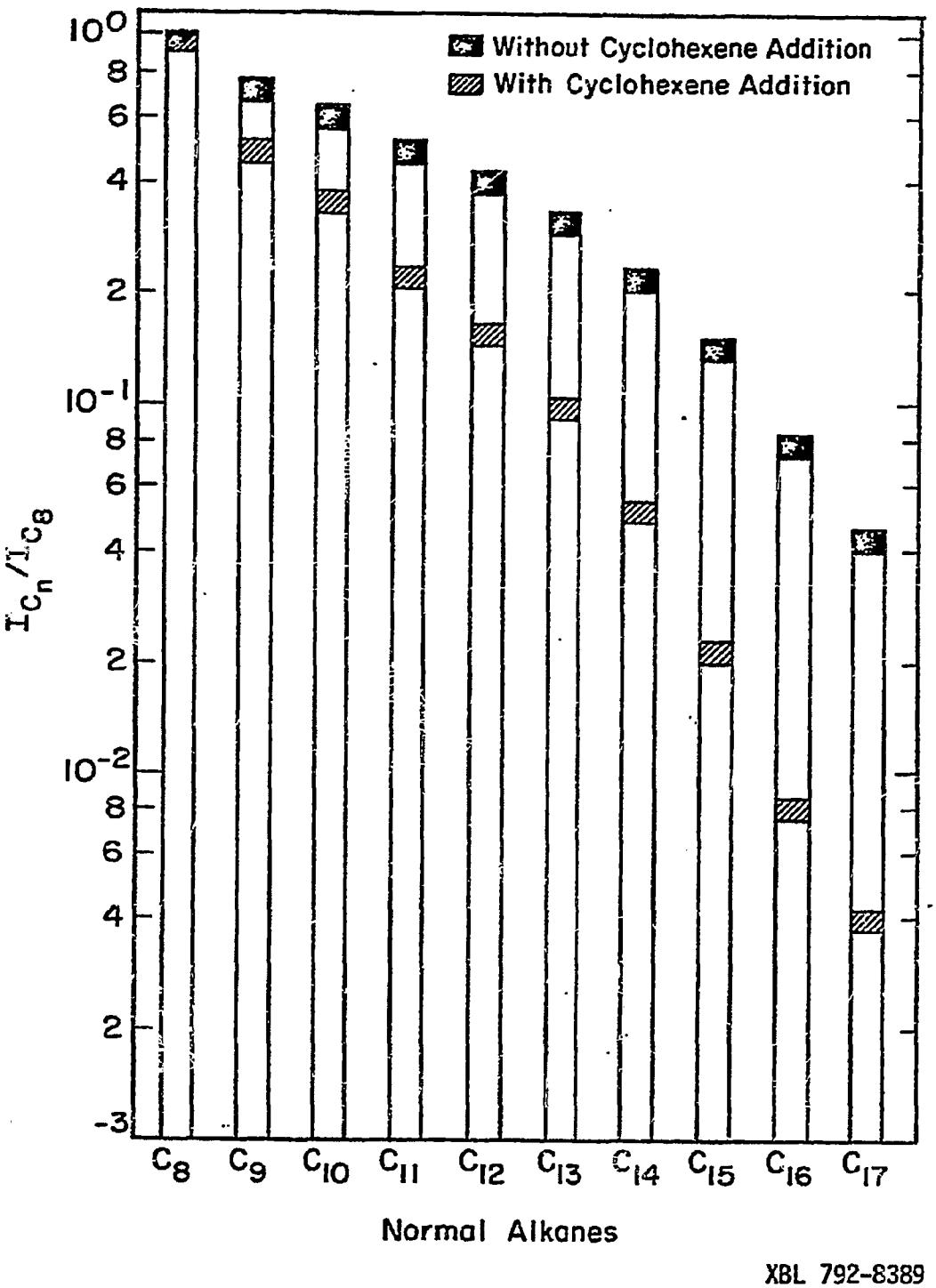

Figure 24. Normal alkane product intensities relative to n-octane versus carbon number

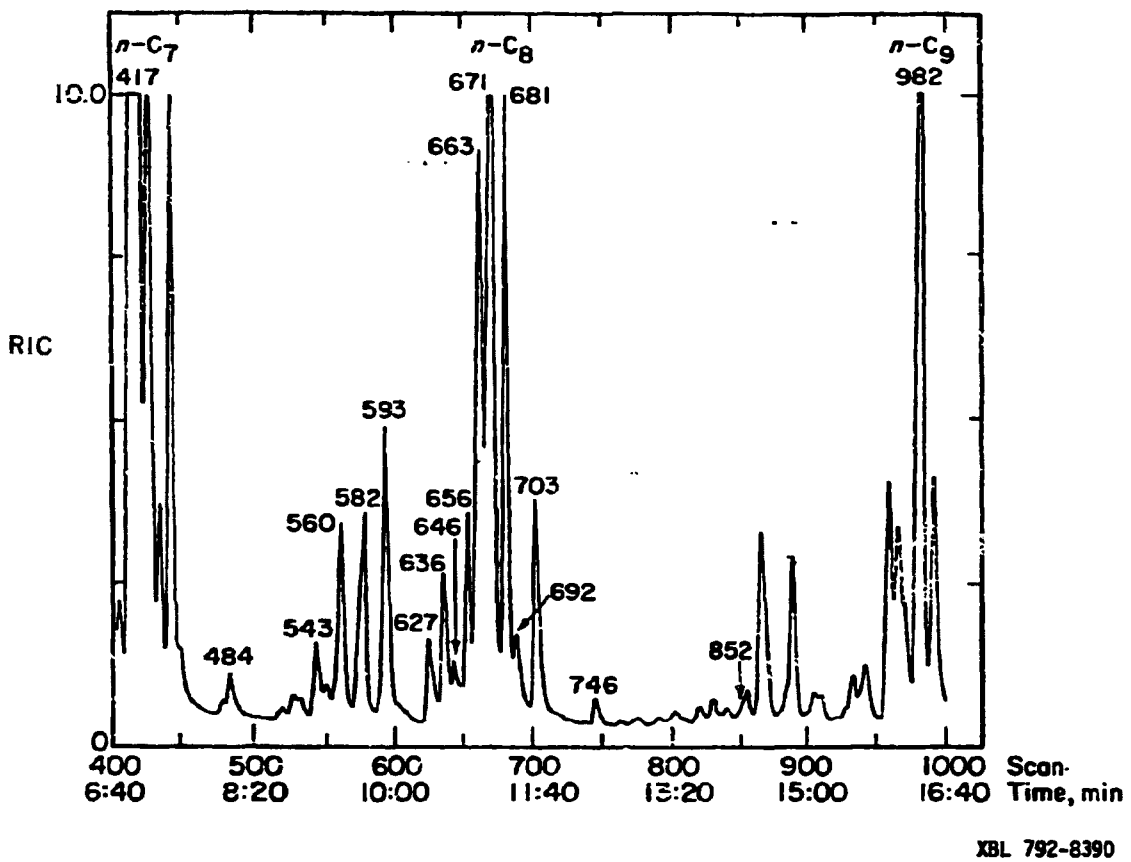

Figure 25. Chromatogram of synthesis products when cyclohexene is present

spectra of known compounds contained in the library of the GC-MS. By this means the peaks at scans 484, 560, and 746 were positively identified as 3-methyl cyclohexene, 1-methyl cyclohexene, and ethyl cyclohexane, respectively. The small peak at scan 852 was identified as 1-ethyl cyclohexene, but the quality of this identification is not as high as that of the fully resolved peaks. Examination of the chromatogram in the region between scans 1000 to 1400 revealed small peaks at scans 1055 and 1385 which could be identified as propyl- and butyl cyclohexane respectively. The intensities of the alkyl cyclohexene and alkyl cyclohexane products are listed in Table 10. It is significant to note that none of the products listed in Table 10 were observed as impurities in the cyclohexene or in the synthesis products collected when cyclohexene was absent from the feed.

A careful examination of the chromatogram was made to determine whether other products such as norcarane, methyl cyclohexane, propyl cyclohexene, and butyl cyclohexene could be identified. No definitive conclusion was reached since in each case the compound was estimated to elute at the same time as one of the synthesis products.

D. Discussion

The present experiments demonstrate that ethylene and cyclohexene will react with carbon containing species present on the Ru catalyst during Fischer-Tropsch synthesis. The important question to be adddressed is whether the

Table 10

Products of Reaction with Cyclohexene

Compound	Peak Intensitties (ion counts)
1-methyl cyclohexene	4.8×10^4
3-methyl cyclohexene	1.5×10^4
1-ethyl cyclohexene[a]	9.1×10^3
ethyl cyclohexane	5.9×10^3
propyl cyclohexane	1.9×10^3
butyl cyclohexane	6.8×10^2

a. Present as a shoulder on the leading edge of a larger peak

products of such reactions can be interpretated as evidence for surface alkylidene groups. To initiate this discussion it is useful to review what is known about the reactions of alkylidenes with ethylene and cyclohexene. Several studies (65,69) have shown that the reaction of gas phase methylene groups with ethylene produces cyclopropane and to a lesser extent propylene. In a similar fashion the reaction of methylene groups with cyclohexene produces norcarane and smaller quantities of 1-, 3-, and 4-methyl cyclohexene. There have been fewer studies of the reactions of olefins with alkylidenes complexed to metals, but what information is available suggests that the products obtained are very similar to those produced in reactions with free alkylidene groups. For example, Fellman et al. (70) have shown that ethylene will react with Ta and Nb-bisneopentylidene to produce 4,4-dimethyl-1-pentene, and Stevens and Beauchamp (68) have noted the formation of norcarane when $CpFe(CO)_2(CH_2)^+$ reacts with cyclohexene.

Based on the available evidence one is led to conclude that cyclopropane and norcarane should be the characteristic products formed by reaction of an adsorbed methylene group with ethylene and cyclohexene respectively. Alternately, one might expect to detect propylene and methyl cyclohexene which are the thermodynamically more stable isomers of cyclopropane and norcarane. Given this perspective, it seems reasonable to propose that the nearly four-fold

increase in propylene production observed during ethylene addition to the feed can be explained by a reaction involving adsorbed methylene groups. This interpretation is further supported by the detection of methyl cyclohexene when cyclohexene is added to the feed.

The observation of ethyl cyclohexene and ethyl, propyl- and butyl cyclohexane may be viewed as further evidence for the presence of adsorbed alkylidenes. The formation of alkyl cyclohexanes most likely proceeds by initial reaction of an alkylidene with cyclohexene and subsequent hydrogenation of the reaction intermediate. It is interesting to observe that the intensities for the alkyl cyclohexane peaks listed in Table 10 decrease as one proceeds from ethyl- to butyl cyclohexane. This pattern parallels the rates of formation of C_2 through C_4 products (71) and is suggestive of a chain growth process involving the polymerization of adsorbed methylene groups.

The participation of adsorbed methylene groups in the mechanism of chain growth on Ru is further supported by the influence of cyclohexene on the distribution of C_8 through C_{17} normal alkanes, presented in Fig. 25. If methylene groups are involved in chain propagation, then a reduction in the surface concentration of these groups could be expected to suppress the formation of higher molecular weight products. Furthermore, the degree of suppression should be greater, the higher the carbon number. These are exactly

the effects produced by the addition of cyclohexene to the synthesis feed.

In summary the present study has provided evidence that alkylidene groups may be present on the surface of a Ru catalyst during Fischer-Tropsch synthesis. The polymerization of methylene groups to form higher molecular weight alkylidenes is also indicated by these results.

V. ACKNOWLEDGMENTS

I am greatly indebted to Professor Alexis T. Bell for his patience, advice and guidance throughout the course for this research. I am also grateful for his counseling in matters beyond the scope of this work which will serve to aid my endeavors for many years to come. I would like to thank Dr. Henry Wise and Professors Gabor Somorjai and Eugene Petersen for their helpful discussions and instruction in the field of catalysis. A special thanks goes to Dr. Amos Newton for performing the GC-MS analysis and for his assistance in interpreting the reams and reams and reams of data.

I would be remiss if I did not extend thanks to my colleagues in the department. Their suggestions and comments, while at times unsolicited and unappreciated, definitely were helpful. While many could be listed, I would like to mention C. Steven Kellner, D'Arcy Lorimer, Gordon Low, Mike Veraa, Wayne Bollinger, Tibor Derencsenyi and Vladimir Kuznetsov.

I would like to thank the many friends I have met and made during my years at Berkeley, who made graduate school an enjoyable experience. I extend specific and special thanks to Martha Dixon for sharing the highs and low of my experiences and supporting me through it all.

Finally, I would like to acknowledge the various private and public agencies which provided my financial

support, DuPont, NSF, and the U.S. Department of Energy.

REFERENCES

1. Y. T. Eidus, Russian Chem. Rev., 36(5), 338(1967).
2. G. A. Mills, and F. W. Steffgen, Cat. Reviews, 8(2). 159 (1973).
3. V. M. Vlasenko, and G. E. Yuzefovich, Russian Chem. Rev. 38(9), 728 (1969).
4. H. Storch, N. Golumbic, and R. Anderson, "The Fischer-Tropsch and Related Synthesis", Wiley, New York, (1951).
5. M. A. Vannice, J. Catal. 37, 449, (1975).
6. R. C. Everson, E. T. Woodburn, and A. R. M. Kirk, J. Catal. 53, 186 (1978).
7. D. L. King, J. Catal. 51, 386 (1978).
8. R. A. Dalla Betta, A. G. Piken, and M. Shelf, J. Catal. 35, 54 (1974).
9. R. A. Dalla Betta, A. G. Piken, and M. Shelef, J. Catal. 40, 173 (1975).
10. F. S. Karn, J. F. Schultz, and R. B. Anderson, I & EC Product R & D, 4(4), 265 (1965).
11. M. A. Vannice, J. Catal. 50, 228 (1977).
12. M. A. Vannice, J. Catal. 37, 462 (1975).
13. C. R. Guerra, J. of Colloid and Interface Sci. (29(2), 229 (1969).
14. M. F. Brown, and R. D. Gonzalez, J. Phys. Chem. 80(15). 1731 (1976).
15. M. F. Brown, and R. D. Gonzalez, J. Catal. 48, 292 (1977).
16. R. A. Dalla Betta, J. Phys. Chem. 79(23), 2519 (1975).

17. C. R. Eady, B. F. G. Johnson, and J. Lewis, J. C. S. Dalton, 477 (1977).

18. R. A. Dalla Betta, and M. Shelef, J. Catal. 48, 111 (1977).

19. D. L. King, Preprints, A. C. S. Div. of Petrol. Chem., 23(2), 482 (1978).

20. A. A. Davydov, and A. T. Bell, J. Catal. 49, 332 (1977).

21. D. W. McKee, J. Catal. 8, 240 (1967).

22. J. McCarty, P. Wentrcek, and H. Wise, SRI-International Menlo Park, CA, personal communication.

23. G. Broden, T. N. Rhodin, C. Brucker, R. Benbow, and Z. Hurych, Surface Sci. 59, 593 (1976).

24. R. B. Levy, and M. Boudart, Science, 181, 547 (1973).

25. G. G. Low, and A. T. Bell, J. Catal. in press

26. J. G. McCarty, and H. Wise, J. Catal. Preprint

27. J. A. Rabo, A. P. Risch, and M. L. Poustma, J. Catal. 53, 295 (1978).

28. R. Ku, N. A. Gjostein, and H. P. Bonzel, Surface Sci. 64, 465 (1977).

29. T. E. Madey, and D. Menzel, Japan J. Appl. Phys. Suppl. 2, Pt. 2, 229 (1974).

30. D. W. Goodman, T. E. Madey, M. Ono, and J. T. Yates, Jr., J. Catal. 50, 279 (1977).

31. F. C. Fuggle, E. Umbach, P. Feulner, and D. Menzel, Surface Sci. 64, 69 (1977).

32. G. Blyholder, and L. D. Neff, J. Phys. Chem. 66, 1464 (1962).

33. G. Blyholder and L. D. Neff, J. Phys. Chem. 66, 1664 (1962).

34. G. Henirici-Olive, and S. Olive, Angew. Chem. Int. Ed. Engl. 15, 136 (1976).

35. G. Blyholder, and P. H. Emmett, J. Phys. Chem. 63, 962 (1959).

36. G. Blyholder, and P. H. Emmett, J. Phys. Chem. 64, 470 (1960).

37. O. Levenspiel, "Chemical Reaction Engineering", Second Ed., John Wiley and Sons, New York, 1972.

38. R. A. Dalla Betta, J. Catal. 34, 57 (1974).

39. K. C. Taylor, J. Catal. 38, 299 (1975).

40. S. R. Craxford, and E. K. Rideal, J. Chem. Soc., 1604 (1939).

41. S. Weller, J. A. C. S. 69, 2432 (1947).

42. S. Weller, J. A. C. S. 70, 799 (1948).

43. J. T. Kummer, T. W. DeWitt, and P. H. Emmett, J. A. C. S. 70, 3632 (1948).

44. J. T. Kummer, H. H. Podgurski, W. B. Spencer, and P. H. Emmett, J. A. C. S. 73, 564 (1951).

45. J. T. Kummer, and P. H. Emmett, J. A. C. S. 75, 5177 (1953).

46. F. M. Dautezberg, J. N. Heller, R. A. Van Santen, and H. Verbeck, J. Catal. 50, 8 (1977).

47. K. J. Singh, and H. E. Grenga, J. Catal. 47, 328 (1977).

48. L. J. Bellamy, "The Infrared Spectra of Complex Molecules", 3rd ed., John Wiley & Sons, New York, 1975.

49. C. R. Guerra, and J. H. Schulman, Surface Sci. 7, 229 (1967).

50. W. A. Bollinger, "Gravimetric Adsorption Study of Hydrogen and Carbon Monoxide on a Supported Ruthenium Catalyst", M. S. thesis, Department of Chemical Engineering, University of California, Berkeley, CA. 1976.

51. H. P. Bonzel, and J. Ku, J. Vac. Sci. & Tech. 9, 663 (1972).

52. J. A. Joebstl, J. Vac. Sci. & Tech. 12, 347 (1975).

53. R. Ducros, and R. P. Merrill, Surf. Sci. 55, 227 (1976).

54. R. L. Palmer, and J. N. Smith, J. Chem. Phys. 60, 1453 (1974).

55. J. N. Smith, and R. L. Palmer, J. Chem. Phys. 56, 13 (1972).

56. S. L. Bernasek, and G. A. Somorjai, J. Chem. phys. 62, 3149 (1975).

57. D. R. Monroe, "The structure and Chemistry of Oxygen Adsorbed on Pt (111) and its Reaction with Reducing Gases", Ph.D. thesis, Department of Chemical Engineering, University of California, Berkeley, Ca. 1977.

58. W. H. Weinberg, and R. P. Merrill, J. Catal. 40, 268 (1975).

59. E. Miyazaki, and I. Yasumori, Surf. Sci. 55, 747 (1976).

60. E. M. Savitskii, V. P. Polyakova, and N. B. Gorina, "Effect of Carbon on the Structure and Properties of Polycrystalline and Single-Crystal Ruthenium".

Vyrashchivanie Monokrist. Tugoplavkikh Redk. Metal., ed. E. M. Savitskii, Nauka, Moscow, 1973.

61. C. Wagner, Adv. Catal. 21, 323 (1970).

62. A. J. Deeming, and M. Underhill, J. C. S. Dalton, 1415 (1974).

63. P. W. Jolly, and R. Petit, J. A. C. S. 88, 5044 (1966).

64. H. Ibach, H. Hopster, and B. Sexton, Appl. Surf. Sci. 1, 1 (1977).

65. W. Kirmse, "Carbene Chemistry", 2nd ed., Academic Press, New York, 1971.

66. M. Hansen, "Constitution of Binary Alloys", 2nd ed., McGraw Hill, New York, 1958.

67. R. B. Calvert and J. R. Shapley, J. A. C. S. 99(15), 5226 (1977).

68. A. E. Stevens, and J. L. Beauchamp, J. A. C. S. 100(8), 2584 (1978).

69. W. B. DeMore, and S. W. Benson, "Advances in Photochemistry", Vol. 2, Ed. W. A. Noyes, Jr., G. S. Hammond, and J. N. Pitts, Jr., Interscience Publishers, New York 1964.

70. J. D. Fellman, G. A. Ruprecht, C. D. Wood, and R. R. Schrock, J. A. C. S. 100(8), 5962 (1978).

71. C. S. Kellner, and A. T. Bell, unpublished results.

APPENDIX I

Determination of Crystallite Size

The metal island, crystallite, is assumed cubic with 5 exposed faces of length L. As discussed by Dalla Betta (38) the average surface area of an exposed Ru atom is 8.17 $\mathring{A}^2$. This leads to:

$$\frac{\text{surface Ru}}{\text{crystallite}} = \frac{5 \times L^2}{8.17\ \mathring{A}^2/\text{surface Ru}} \qquad (1)$$

where L = $\mathring{A}$

If the density of the crystallite is the same as the density of bulk ruthenium metal:

$$\frac{\text{molecules Ru}}{\text{crystallite}} = L^3 \times (7.27\text{x}10^{-2}\text{molecules Ru}/\mathring{A}^3) \qquad (2)$$

The dispersion, D, is defined by

$$D = \text{surface Ru/total Ru} \qquad (3)$$

Equations (1), (2) and (3) are combined and rearranged to give

$$L = \frac{5}{D \times (8.17) \times (7.27\text{x}10^2)} \qquad (4)$$

Using the dispersion measured by hydrogen chemisorption and Equation (4) a crystallite size can be calculated.

U.S.GPO:1979-689-058 (F) 26

U.S. DEPARTMENT OF COMMERCE
Technology Administration
National Technical Information Service
Springfield, VA 22161 (703) 605-6000